



UNIVERSITY OF LEEDS

This is a repository copy of *Temporal and spatial changes in style of accretion at the bend of a sinuous turbidite slope channel (channel–levee Complex 5, Tachrift System of NE Morocco)*.

White Rose Research Online URL for this paper:

<https://eprints.whiterose.ac.uk/id/eprint/224977/>

Version: Accepted Version

Article:

Marini, M., Pantopoulos, G., Invernizzi, D. et al. (3 more authors) (2025) Temporal and spatial changes in style of accretion at the bend of a sinuous turbidite slope channel (channel–levee Complex 5, Tachrift System of NE Morocco). *Journal of Sedimentary Research*, 95 (2). pp. 286-313. ISSN 1527-1404

<https://doi.org/10.2110/jsr.2024.052>

This item is protected by copyright. This is an author produced version of an article published in the *Journal of Sedimentary Research*. Uploaded in accordance with the publisher's self-archiving policy.

Reuse

Items deposited in White Rose Research Online are protected by copyright, with all rights reserved unless indicated otherwise. They may be downloaded and/or printed for private study, or other acts as permitted by national copyright laws. The publisher or other rights holders may allow further reproduction and re-use of the full text version. This is indicated by the licence information on the White Rose Research Online record for the item.

Takedown

If you consider content in White Rose Research Online to be in breach of UK law, please notify us by emailing eprints@whiterose.ac.uk including the URL of the record and the reason for the withdrawal request.



eprints@whiterose.ac.uk
<https://eprints.whiterose.ac.uk/>

Temporal and spatial changes in style of accretion at the bend of a sinuous turbidite slope channel (channel–levee Complex 5, Tachrift System of NE Morocco)

Mattia Marini,^{1*} George Pantopoulos,¹ Daniele Invernizzi,¹ Fabrizio Felletti,¹ Imad El Kati,² and Adam McArthur³

¹ Dipartimento di Scienze della Terra “A. Desio”, Università degli Studi di Milano, Milan, Italy

² Natural Resources and Environment laboratory, Polydisciplinary Faculty of Taza, Sidi Mohamed Ben Abdellah University, Taza, Morocco

³ School of Earth and Environment, University of Leeds, Leeds, LS2 9JT, United Kingdom

**Corresponding author: mattia.marini@unimi.it*

Keywords: *outcrop, meandering channel, lateral-accretion package, counter bar, outer-bank bar, turbidity currents*

Abstract

This outcrop study describes variously accreted deposits constituting the fill of a sinuous channel from the Tachrift System (Upper Miocene of the Taza–Guercif Basin, NE Morocco). Detailed correlation of fifty-nine logs from three outcrops spanning a left-turning bend allowed recognition of four stratigraphic units recording channel establishment and levee development, aggradation and bend translation and expansion, and switching of the parent channel. Results show that lateral-accretion packages (LAPs) formed at the inner bank represent the main intra-channel depositional element, co-occurring with equally sandstone-rich and coarse-grained deposits accreted at the outer bank. The best-exposed and larger example of LAPs occurs in two correlated exposures c. 500 meters apart alongstream, which most likely straddle the bend apex. In the upstream outcrop, cut-and-fill features and sandstone amalgamation make it difficult to recognize the lateral accretion. Here, LAPs consist of bedsets of amalgamated sandstones bounded by thalweg-dipping erosional surfaces that are lined up with mud-clast breccias in the deeper part of the channel fill. In the downstream outcrop, the correlated LAPs become lithologically more layered along most of their

profile. Moving up the accretion dip, to the LAP top, they comprise finer-grained, and more structured sandstones alternating with mudstones. In the downstream outcrop, LAPs transition into a mud-rich heterolithic deposit characterized by trough-cross inclined stratification, which dips at a high angle to mean downstream paleocurrent. This deposit extends over a distance of a few hundred meters, straddling the inner- to outer-bank transition, and is interpreted as the expression of bank-attached bars (here termed turbidite counter-bars) forming in a flow separation zone and are. This study provides insights into longitudinal heterogeneity of LAPs and lithological composition of outer-bank bars and turbidite counter bars never before observed at outcrop.

INTRODUCTION

Submarine channels and associated levees are bathymetric features of the seafloor formed by the action of turbidity currents and other types of sediment gravity flows (Menard, 1955; Mutti and Normark, 1987, Normark and Piper, 1991; Janocko et al., 2013a; Peakall and Sumner, 2015). Based on similar planform patterns, turbidite channels have been often paralleled to fluvial channels, despite obvious differences in terms of flow types and kinematics (Das et al., 2004; Kevil et al. 2006; Peakall et al., 2007; Wynn et al., 2007; Janocko et al., 2013a, 2013b; Peakall and Sumner, 2015; Jobe et al., 2020; Fukuda et al., 2023) and sedimentary products (Jobe et al., 2016). Similarly to fluvial channels, turbidite channels can be sinuous and modify their sinuosity to adjust to changes in flow conditions (Peakall et al., 2000; Kneller, 2003). An increase in channel sinuosity is typically accompanied by channel-bend expansion (e.g., swing) and incremental channel cross-sectional asymmetry (e.g., Reimchen et al., 2016). This cross-sectional asymmetry is accompanied with an uneven distribution of sediment accumulation and erosion across the channel, which in turn reflects the helical character of flow through sinuous channels (Fukuda et al., 2023). Present understanding of this helical flow suggests that it arises mainly from combination of the curvature-induced vertical variation of centrifugal forces and super-elevation of density interfaces towards the outer bank (Peakall and Sumner, 2015; Arnott et al., 2021; Wells and Dorrell, 2021). This sets up the conditions for formation of laterally accreted, bank-attached bars similar to fluvial point bars. These deep-marine point bars span a range of scales (Elliott, 2000b; Abreu et al, 2003; Wynn et al., 2007; Janocko et

al., 2013a, 2013b) and their deposits are commonly referred to as lateral-accretion packages (hereafter LAPs).

However, conspicuous sediment accumulations have been also documented at the outer bank in the form of either mounded (e.g., nested mounds; Phillips, 1987; Timbrell, 1993; Peakall et al., 2000) or wedge-shaped deposits (e.g., outer-bank bars; Nakajima et al., 2009), and in the transition between the inner bank and the outer bank of the following bend (oblique accretion deposits of Straub et al., 2011 and inner- to outer-bank transition bars of Janocko et al., 2013b), suggesting that there is more complex pattern to deposition in sinuous turbidite channels.

Despite point bars and outer-bank bars being widely recognized as major intra-channel architectural elements of turbidite systems (Abreu et al., 2003; Nakajima et al., 2009), their sedimentary heterogeneity is still relatively poorly documented (Abreu et al., 2003; Arnott 2007; Wynn et al., 2007; Dykstra and Kneller, 2009; Kane et al., 2010) and their formative processes are not fully understood (Das et al., 2004; Keevil et al., 2006; Peakall et al., 2007; Janocko et al., 2013b).

Outcrop studies can help resolve this knowledge gap, by providing insights into geometry and sedimentary composition of these bar deposits (e.g., Elliott, 2000b; Arnott 2007; Janbu et al., 2007; Dykstra and Kneller, 2009; Cronin et al., 2000; Pantopoulos et al., 2025). As such, outcrop data are useful for better constraining process modelling (Das et al., 2004; Keevil et al., 2006; Peakall et al., 2007; Janocko et al., 2013b) and subsurface characterization of channel fills (Abreu et al., 2003; Janocko et al., 2013a).

Along with companion paper Pantopoulos et al. (2025) in this issue, which quantifies the internal heterogeneity, this work documents the sedimentary architecture of a channel–levee complex (Complex 5) belonging to the Tachrift System (Upper Miocene of the Taza–Guercif Basin, NE Morocco) (Felletti et al., 2020, 2023). The c. 20-m-thick lower and sand-rich part of Complex 5 was investigated by acquiring and correlating fifty-nine closely spaced sedimentary logs (with average spacing of c. 50 m), which yielded three variously oriented transects through the deposits accumulated across the evolving bend of a leveed channel. The aim of this work was three-fold: i) to document the stratigraphic and spatial variability of depositional style across the bend of a sinuous

slope channel; (ii) to detail the sedimentary facies associations characterizing the deposits accumulated in specific regions of the channel bend and compare them with published depositional models from literature, and (iii) to provide insights into likely controls on stratigraphic changes in channel trajectory and depositional style.

GEOLOGICAL SETTING

Together with the Gharb and Fes–Meknes Basins (Fig. 1A), the Taza–Guercif Basin of NE Morocco (Fig. 1A) forms the Rifian Corridor (Flecker et al., 2015; Capella et al., 2018), a remnant of the Rif foreland-basin system (Bernini et al., 1999; Sani et al., 2000), which acted as a seaway connecting the Atlantic Ocean to the Mediterranean Sea during the Late Miocene (De Weger et al., 2021; Capella et al., 2017, 2019). The Taza–Guercif Basin was established in the Tortonian as the result of flexural loading by the advancing Rif thrust sheets and reactivation of Middle Atlas structures (Bernini et al., 2000; Sani et al., 2000; Capella et al., 2017). The basin fill sits on top of a regional-scale unconformity recording the Cretaceous to Early Miocene compressional reactivation of Jurassic extensional faults of the Middle Atlas (Bernini et al., 1999; de Lamotte et al., 2009) and started with alluvial conglomerates, sandstones, and mudstones of poorly constrained Tortonian age, representing the Draa Sidi Saada Formation (Figs. 1B and C).

In the late Tortonian, subsidence resulted in a marine transgression (Krijgsman et al., 1999) and deposition of a deepening-upwards succession of alternating shelfal sandstones, carbonates, and hemipelagic marlstones representing the Ras el Ksar Formation (Figs. 1B, C; Benzaquen, 1965; Bernini et al., 2000; Gelati et al., 2000). Further drowning established widespread hemipelagic sedimentation in the Rifian Corridor with accumulation of the marlstone-rich Melloulou Formation, which is up to several hundreds of meters thick (*Marnes Bleues* in Benzaquen, 1965; *Marnes Tortoniennes* in Colletta, 1977). The Melloulou Formation is locally intercalated with turbidite-rich packages (Gelati et al. 2000; Sani et al. 2000), like those making up the El Rhirane System and the Tachrift System exposed in the southernmost part of the basin fill (Fig. 1B), which were fed from the south with sediments supplied from the Middle Atlas (Gelati et al. 2000; Pratt et al., 2016; Felletti et al., 2020).

In the early Messinian, tectonic closure of the Rifian Corridor was followed by shallowing and subsequent emersion of the Taza–Guercif Basin (Krijgsman et al., 1999; Krijgsman and Langereis, 2000), resulting in a sedimentary progression from marlstones with gypsum (the Gypsiferous Marls Subunit, Fig. 1C) to shallow marine and continental deposits (the Kef Ed Debe Formation, Fig. 1C; Gelati et al., 2000).

The Tachrift System

The Tachrift System is exposed to the east of the Zobzit River, in a c. 600-m-thick section (hereafter the Zobzit Section; Fig. 1C) comprising numerous alternating turbidite-rich (eighteen, according to Krijgsman et al., 1999) and marlstone-rich packages, each up to a few tens of meters thick (Gelati et al., 2000). Magnetostratigraphic investigations (Krijgsman *et al.*, 1999; Krijgsman and Langereis, 2000) indicate that the Zobzit Section was deposited between 7.7 and 7.2 Ma, with an accumulation rate that increased over time from 0.4 m/kyr (latest Tortonian) to 1.7 m/kyr (earliest Messinian). Felletti *et al.* (2020) recently mapped the Tachrift System as nine channel–levee turbidite complexes (*sensu* Sprague et al., 2005) and interpreted them as the product of as many subsequent channel belts traversing the southern slope of the Taza–Guercif Basin. Among these, the c. 50-m-thick Complex 5 occurs half-way within the Tachrift System and straddling the boundary between the reverse polarity Chron C3Br.2r and the normal polarity Chron C3Br (Fig. 1C) (Krijgsman and Langereis, 2000).

In the study area, Complex 5 shows a largely bipartite stratigraphy, consisting of a lower sand-rich channel-fill body up to c. 20 m thick (hereafter referred to as the main sandstone body) and an upper marlstone-rich package comprising three thin-bedded turbidite bedsets (Fig. 2A), each up to a few meters thick. Geological mapping indicates that the main sandstone body is replaced eastwards by mud-rich heterolithics, earlier recognized as levee deposits (Felletti et al., 2020) (Fig. 2A).

MATERIAL AND METHODS

The stratigraphy and sedimentary architecture of the main sandstone body of Complex 5 was evaluated correlating fifty-nine sedimentary logs (with average spacing of c. 50 m) from three

outcrops (Figs. 2A, 3) hereafter referred to as the North Outcrop, the Southwest Outcrop, and the Southeast Outcrop. Logging was extended upwards so as to include the oldest two of the three thin-bedded turbidite bedsets (hereafter TBT1–2) occurring in the marlstone-rich package above the main sandstone body (Figs. 2A, 3), which, being exposed in most localities, represent useful stratigraphic markers.

True (non-decompacted) thicknesses were measured using a Jacob's staff for long-range measurements and a tape measure for individual beds. For Jacob's-staff measurements, the bedding dip direction and dip of beds with flat geometry (e.g., the cm-thick beds in the marlstone immediately below the main sandstone body) was used (Fig. 2B). The utilized Jacob's staff (Patacci, 2016), is equipped with a laser pointer able to rotate in the plane of bedding, a feature that was used to verify continuity of bedding surfaces and thus identify inclined strata.

Sedimentary descriptions were made at cm-scale resolution and included lithology, chart-aided estimation of grain size and sorting, sedimentary structures, paleoflow directions from sole casts and sedimentary structures, bioturbation index (after Taylor and Goldring, 1993), and trace-fossil ichnogenus, when this could be determined.

Logs were correlated by walking out laterally continuous beds between adjacent log localities. Correlation panels (Fig. 3A–C) were then constructed flattening logs and correlations to datum planes that can be reasonably assumed to have been nearly flat at the time of deposition. The base of a distinctive bedset occurring close to the bottom of the main sandstone body was used as a primary datum in the North Outcrop and the Southwest Outcrop. Where the primary datum is not present or exposed (e.g., in the Southeast Outcrop and in the North Outcrop, to the south-southeast of log 28 and in a few localities to the west-northwest of log 9A; Fig. 3A), the top of TBT1 was used as an alternative datum. Based on the observation that the stratigraphic distance (c. 15 m) between the primary datum and TBT1 shows only minor changes (less than 20%) at localities in which they are both exposed, the top of TBT1 was also taken as a flat datum upon which the correlation panels obtained for each outcrop were hung (Fig. 3A–C). Hence, these datums allowed construction of a 3D fence diagram across the study area (Fig. 2A).

Five major stratigraphic surfaces were defined based on major vertical changes in sedimentary facies and facies associations. These surfaces bound four stratigraphic units, labelled Unit 1 to 4 from older to younger (Fig. 3A–C), each composed of one or more architectural elements (e.g., channel fills, levees, crevasse splays) and recording a distinct phase of channel evolution.

Terminology

Throughout this paper, reference to channel bends, their regions, and the associated deposits is made using the terminology clarified in Figure 4. Bends are referred to as right-turning and left-turning based on their curvature direction defined looking downstream. Inner and outer are respectively used to refer to the point bar side of a bend and to the cut bank side of a bend. The bend apex is the point of maximum curvature, which separates an upstream region from a downstream region of the bend. Two subsequent (opposite) bends are separated by a transition zone, a relatively broad area where channel curvature gradually changes direction across the so-called inflection point. The term *bar* is used to refer to a constructional (depositional) macroform having a length of the same order as the channel width and displaying positive topographic expression relative to the channel thalweg (Nakajima et al., 2009). Following Janocko et al. (2013b), bank-attached bars are termed *point bars*, *outer-bank bars*, and *inner- to outer-bank* and *outer- to inner-bank transition bars*, depending on their position relative to banks (Fig. 4). The position of inner- to outer-bank transition bars is similar to that of fluvial counter bars. Outer-bank bars can be further distinguished into *up-apex* and *down-apex*.

Bedsets having original (depositional) inclined stratification interpreted as formed from lateral growth of a point bar will be referred to as a lateral-accretion package (LAP).

Since most bank-attached bars have a sigmoidal profile orthogonal to channel axis (Elliott, 2000b; Abreu et al., 2003; Dykstra and Kneller, 2009; Nakajima et al., 2009), the bedsets constituting their deposit can be ideally subdivided into three main segments: the topset is the upper flat-lying part of the sigmoid, which ends onto the bank; the middleset encompasses the relatively thicker-bedded and most (thalweg-ward) inclined part of the sigmoid; the toset constitutes the down-lapping part of the sigmoid, ending in the thalweg.

Lastly, the terminology of Kane and Hodgson (2011) is adopted to refer to levee parts and sub-environments: *inner levee* is used to describe the (channel-facing) part of the levee between the channel thalweg and the levee crest; *outer levee* describes that part of the levee between the levee crest and its distal termination.

RESULTS

Outcrop Description, Stratigraphy, and Large-Scale Architecture

The studied outcrops are cut by several high-angle reverse faults (Fig. 2A), which exhibit slickensides with vertical striations and are related to Plio-Quaternary deformation of the Taza–Guercif Basin (Bernini et al., 1994; Sani et al., 2000; El Kati et al., 2022). The largest of these faults (hereafter fault α) dips to the north-northwest and cuts the Southwest Outcrop (Figs. 2A, 5C) and the Southeast Outcrop (Fig. 2A) with a stratigraphic throw in excess of c. 10 m. Fault α is in turn cut by a northeast-dipping reverse fault (hereafter fault β) with a vertical throw that varies from less than a few meters in the north (between logs 3 and 3A; Fig. 6D), to c. 10 m in the south (between logs 60 and 41).

The main sandstone body is exposed in all studied outcrops, with variable thickness, degree of amalgamation, and facies composition, overlying the c. 10-m-thick marlstone-rich package that separates it from Complex 4 (Figs. 2A, 6D).

In the Southwest Outcrop, the main sandstone body is c. 15 m thick (log 67, Figs. 3B, 5A) and comprises all of the recognized stratigraphic units, albeit Unit 4 is locally absent due to modern erosion (e.g., between log localities 63 and 60), or covered by a relatively thick soil (e.g., log locality 67). Units 1–3 are more coarse-grained and amalgamated than elsewhere, and their deposits can be seen to pass eastwards into mud-rich heterolithics, earlier recognized as levee deposits (Felletti et al., 2020), before they are cut by fault α (Fig. 5C).

In the North Outcrop the main sandstone body is up to c. 17 m thick (log 27, Fig. 6A, B) and becomes thinner (less than c. 10 m in log 5; Fig. 6D), muddier, and less amalgamated (Fig. 6C, D) towards

the northwest. Similar to the Southwest Outcrop, correlations in the North Outcrop demonstrate that the sand-rich deposits of Units 1-3 transition eastwards (e.g., between logs 27 and 33; Fig. 3A) into levee deposits, and that Unit 4 northwestward from log locality 28A is heterolithic and increasingly mud-rich.

The Southeast Outcrop is involved in the damage zone of fault α and thus is locally poorly exposed (e.g., between log localities 39 and 41, Fig. 2A). Correlations show that most of the main sandstone body belongs to Unit 4 and thins towards the northwest and towards the east (between logs 35 and 36 and logs 41 and 42, respectively; Fig. 3A, C), where it is replaced by levee deposits.

In light of the north- northeast-directed paleocurrent interpreted from sole casts (Fig. 2C), which is similar to that of the sandwiching channel–levee complexes 4 and 6 (Reguzzi et al., 2023; Zuffetti et al., 2023), the gross distribution of channelized vs. levee deposits of Complex 5 (Fig. 3A–C) is indicative of a relatively stable channel pathway during deposition of Units 1–3, and a late phase of eastward channel switching (Unit 4).

Sedimentary Facies and Facies Associations

Seven sedimentary facies (labelled F1 to F7; Fig. 7) were identified in Complex 5 based on lithology, grain size, and sedimentary structures, and related to the classical facies schemes of Bouma (1962), Lowe (1982), and Mutti (1992) (Table 1).

Sedimentary facies were then grouped into seven facies associations (labelled FA1 to FA7), which are unique in terms of lithological and sedimentary facies fractions, grain size ranges and bed thickness, and stratification character (Fig. 8). As illustrated by several key exposures (Figs. 9, 10) and bed-by-bed correlations (e.g., Figs. 11–13), these facies associations occur in a predictable order across each of the four units of Complex 5 and can thus be interpreted as parts of channel-fill and levee elements (Fig. 8).

Facies Association 1 (Mud-Clast-Rich Channel-Fill Sandstones)

Occurrence and description.--- Facies Association 1 (FA1) is the coarsest and most sandstone-rich deposit of Complex 5. It is present in all units except in Unit 1 (Figs. 11–13) and is relatively more abundant in the Southwest Outcrop southeast of log 65 (Figs. 11D, 12D), where it is locally associated with basal erosions a few meters deep and a few hundreds of meters wide (e.g., Fig. 5B). Both in the Southwest Outcrop and in the North Outcrop, FA1 transitions eastwards to FA5 (Figs. 9B, 11–13) and westwards to FA2 (Figs. 9D, 11–13).

FA1 is represented by amalgamated bedsets, up to several meters thick (Figs. 9A, B), dominantly made up of mud-clast-rich coarse sandstones (F1) and, in descending order of abundance, the finer-grained cross-stratified F3 and the structureless to laminated F4 and F5. FA1 bedsets frequently show basal scours up to c. 1 metre deep and a few tens of metres wide, which are locally lined up by discontinuous F2 beds up to several tens of cm-thick.

Bioturbation is absent to low in FA1 (Taylor and Goldring, 1993), with the most frequent trace fossil being represented by *Ophiomorpha* and *Rhizocorallium*.

Interpretation.--- This facies association is an assemblage of S1–S3 of Lowe (1982) and, secondarily, variously developed Bouma (1962) sequences. The generally coarse, poorly sorted, and structureless nature of the deposit, associated with deep basal scouring, suggest rapid deposition from the lower, denser, and more erosive part of high-density flows within the thalweg (e.g., channel axis facies of McHargue et al., 2011).

Facies Association 2 (Trough-Cross-Stratified Channel-Fill Sandstones)

Occurrence and description.--- Facies Association 2 (FA2) constitutes most of the Southwest Outcrop north of log locality 65 (Figs. 9D, 11D, 12D) and is present at various stratigraphic levels in the North Outcrop and in the Southeast Outcrop (Figs. 11-13), most commonly interbedded with the muddier FA3 and FA4 (Figs. 11-13, 14B). FA2 passes eastwards into the coarser-grained thalweg FA1 (e.g., logs 30–31 and logs 66–65, Figs. 11B, 12C) or into channel-margin (FA5) and/or proximal overbank (FA6) facies associations (logs 23–26, Fig. 11B). Northwestwards and downcurrent, FA2

sandstone become less amalgamated, transitioning into the muddier FA3 and FA4 (logs 26 and 17; Fig. 12B).

It consists of amalgamated bedsets, 0.5 to 2 m thick, of cross-stratified medium sandstones (F3) and structureless medium–fine sandstones (F4), sometimes capped by laminated fine–very fine sandstones (F5) and/or a turbidite mudstone (F6). Bedsets may show a thinning- and fining-upward organization and are frequently erosionally based with scours up to few tens of cm deep and a few meters wide (Figs. 9D, 10A), locally associated with mud-clast breccias (F2) up to a few tens of cm thick (Fig. 7D).

Stratification is curved, subparallel to nonparallel, and inclined (Figs. 9C-E), a character best expressed on outcrop faces oriented at high angle to mean paleocurrent direction. The internal stratification of each bedset shows quite uniform dip and inclination angle (Fig. 9D). In favorable exposures providing a 3D view of the deposit (Fig. 9E), the dip direction of the inclined stratification can be seen to vary within a broad range from one bedset to another, which explains the trough-cross stratified structure of most FA2 exposures. Bioturbation is absent to low.

Interpretation.--- The inclined stratification and the sedimentary-facies composition of FA2, along with its occurrence relative to the coarser-grained thalweg deposits of FA1, suggest that it represents the product of lateral accretion of bank-attached bars, developed beneath high-density turbidity currents.

Facies Association 3 (Sand-Rich Channel-Fill Heterolithics)

Occurrence and description.--- Facies Association 3 (FA3) represents a significant fraction of the North Outcrop northwest of log 27 and of the lower part of Unit 1 in the Southwest Outcrop (Figs. 11A, 12B). It forms packages 1–4 m thick and occurs laterally to and in stratigraphic alternation with the mud-rich heterolithics of FA4 (Figs. 10A, B, 14A) and, locally, with FA2 (e.g. Figs. 11A, 12B, 14B).

The sandstone fraction of FA3 is generally > 50% and consists of beds 20–35 cm thick of structureless to laminated medium–very fine sandstones (F4 and F5). Sandstone beds most

commonly alternate with 1–5-cm-thick turbidite mudstones (F6), but can locally amalgamate (Fig. 10A, B). In E–W outcrop faces (i.e., nearly perpendicular to mean paleocurrent), most beds show sigmoidal profiles and form bedsets with parallel to subparallel inclined stratification and quite homogeneous dip (Fig. 10A). The dip of the inclined stratification changes from one bedset to another, but where it could be measured, it is at a high angle to mean paleocurrent direction and towards eastern quadrants. Conversely, in N–S outcrop faces (perpendicular to the dip of the inclined stratification and nearly parallel to mean paleoflow) beds and bedsets show a variety of lenticular shapes exhibiting compensational or offset stacking, which imparts a trough-cross-stratified character to the deposit (Fig. 10B). Bioturbation is sparse to low.

Interpretation.--- FA3 is an assemblage of sedimentary facies deposited by a range of high- to low-density waning turbidity currents. The laterally accreted nature FA3, along with its local association with the FA2 bar deposits, is suggestive of deposition in bank-attached bars, either in relatively less energetic regions of the bank (e.g., high on the bank profile or in the inner bank, downcurrent from the bend apex) or during phases of reduced sediment input.

Facies Association 4 (Mud-Rich Channel-Fill Heterolithics)

Occurrence and description.--- Facies Association 4 (FA4) is widespread, although the best exposures are those of Unit 3 in the North Outcrop northwest (and downcurrent) of log 18 (Figs. 10A, B, 12). It forms packages 0.5–3 m thick and occurs laterally to and sandwiching the sand-rich heterolithic bars of FA3 (Figs. 10A, B, 11-13).

The sandstone fraction of FA4 is generally less than c. 50% and consists of beds, 5–10 cm thick, of laminated fine-grained sandstones (F5), which alternate with 10–25-cm-thick turbidite mudstone beds (F6) forming parallel-stratified heterolithic bedsets with low-angle-inclined stratification. In several outcrops, FA4 was observed to occur both down- and up-accretion dip of FA3 bars (Fig. 10A) and in the up-accretion dip of FA2 bars (e.g., logs 29 and 27; Fig. 12B). Bioturbation can be up to high, with common *Ophiomorpha*, *Scolicia*, and *Rhizocorallium* burrows.

Interpretation.--- The facies composition and spatial relationship with the sandier FA2 and FA3, suggest that FA4 was deposited either by the upper low-density part of flows in the topset of laterally accreted bank-attached bars (e.g., FA2 point bars or FA3 bars), or in their toeset, during flow waning stages. A similar explanation was provided by Dystra and Kneller (2009) for explaining facies and grain-size trends along the dip of laterally accreted bedsets in the Rosario Formation of Baja California, Mexico.

Facies Association 5 (Channel-Margin Deposits)

Occurrence and description.--- Facies Association 5 (FA5) is limited to the eastern margins of Units 1–3 channel fills (e.g., Figs. 9A, B), where it marks the transition between the channel-filling deposits of FA1-4 and muddier proximal overbank deposits (FA6) (Figs. 11, 12).

FA5 is rather heterogeneous (Figs. 10C, D) in that it shows rapid lateral changes in sandstone fraction and degree of sandstone amalgamation moving eastwards and away from the channel (Fig. 9B). It consists of amalgamated to non-amalgamated sandstone beds, 5–15 cm thick, of structureless medium–fine sandstones (F4) and laminated fine–very fine sandstones (F5), locally capped with sharp or gradational contact by turbidite mudstone beds (F6) up to 5 cm thick (Figs. 10C-D). Sandstone beds are generally sharp- and flat-based, normally graded, and locally enriched in mm-sized, angular to subrounded clasts of turbidite mudstone (Fig. 10D), which can occur close to bed bases but are more commonly found in between the structureless and the laminated parts of beds. Bioturbation is absent to sparse.

Interpretation.--- The occurrence of FA5, that is, at the transition between channel-fill and the proximal overbank deposits of FA6, is indicative of deposition in a channel-margin setting (McHargue et al., 2011). Local enrichment in small mud clasts is interpreted to reflect enhanced substrate erosion due to flow interaction with the channel-facing part of a relatively mud-rich levee.

FA6 (Proximal Overbank Deposits)

Occurrence and description.--- Facies Association 6 (FA6) is exposed in several key localities, bounding the main sandstone body to the east (Figs. 10E, 11-13), and comprising most of Unit 4 in the North Outcrop northwest of log locality 27 (Fig. 13A).

The sandstone fraction of FA6 is generally less than 25% (Fig. 8) and consists of normally graded fine–very fine sandstone beds (F5) less than c. 5 cm, which alternate with 5–25 cm thick beds of turbidite mudstones (F6) and, subordinately, marlstones (F7). Sandstone beds are typically well-cemented and up to moderately bioturbated (Taylor and Goldring 1993), and their top ornamented with well-preserved *Scolicia* and *Rhizocorallium*, and more rarely, *Planolites* burrows (Fig. 7H). Given its generally poorly exposed nature, it was not possible to establish the degree of bioturbation of the mudstones.

Interpretation.--- Sedimentary facies composition and relationship with channel-fill facies associations suggest that FA6 is the product of overbank deposition in a channel-proximal levee setting.

FA7 (Hemipelagic and Distal Overbank Deposits)

Occurrence and description.--- Facies Association 7 (FA7) encapsulates the main sandstone body and TBT1–2 (Figs. 3, 10E, 13A) and was locally observed to pass laterally to FA6 (e.g., logs 26–29; Fig. 11B). It is composed of variable proportions of siliciclastic mudstones (F6) and marlstone (F7), sparsely intercalated with cm-thick normally graded beds of laminated fine–very fine sandstones (F5). Due to its composition, FA7 is prone to rapid weathering and badland topography, and thus is generally poorly exposed, which makes it difficult to establish relative proportions of F6 and F7. Due to its composition, this FA is generally poorly exposed, making it difficult to establish the degree of bioturbation.

Interpretation.--- Sedimentary-facies composition of FA7 suggests that it represents the product of hemipelagic and turbiditic sediment accumulation in a slope environment, at times of reduced sediment input and/or away from contemporaneous turbidite channels.

3D Stratigraphic Organization

The 3D stratigraphic organisation of Units 1–4 is illustrated by the fence diagrams of Figures 11–13, which were built based on physical correlations or inferred from stratigraphic position relative to the TBT1 datum plane. The following sections provide a detailed description of each unit, proceeding from the most upstream to the most downstream outcrop.

Unit 1

Unit 1 is exposed in the Southwest Outcrop and in the North Outcrop (Fig. 11A) and was recognized based on its stratigraphic position, namely above the FA7 mudstones separating it from Complex 4 and below the coarser-grained and more amalgamated Unit 2. It is up to c. 5 m thick and is bounded above by the base of Unit 2, which in the Southwest Outcrop is associated with an erosional surface up to 2 m deep.

Southwest Outcrop.--- In this outcrop, Unit 1 is chiefly made of amalgamated sandstones (Fig. 9D), which makes it impractical to subdivide it further into component bedsets. Nonetheless, a lower finer-grained heterolithic part, in which FA3 is dominant, can be distinguished from an upper part consisting of amalgamated bedsets of FA2 trough cross-stratified sandstones (e.g., logs 68–66A; Fig. 9D). Both in the lower and in the upper and sandier parts of the unit, the inferred direction of accretion of FA2 bedsets is dominantly towards the east-southeast (Fig. 11D).

To the east of locality 63, Unit 1 is poorly exposed, but spot outcrops suggest it is composed dominantly of the mudstone-rich FA6 overbank deposits (Figs. 9B, 11D).

North Outcrop.--- In this outcrop, Unit 1 is relatively mud-rich and well-stratified, which allows identification of seven largely fining- and thinning-upwards bedsets up to c. 2 m thick (marked with Roman numerals I–VII in Fig. 11B). The unit begins between logs 12 and 20 with two erosionally based sandstone bedsets (marked with I and II in Fig. 11B), up to c. 0.50 m thick, which fringe laterally over a scale of a few tens of meters (Fig. 11B), passing into proximal overbank deposits (FA6). A north-northwest-directed flute cast and one north–south-oriented groove cast from the base of bedset II (logs 15–16, Fig. 11A) suggest that paleocurrent was toward northern quadrants.

Upwards in the section, Unit 1 continues with the thicker and more extensive bedsets III–VII, which share a similar laterally accreted internal organization. Where thickest, bedsets III–VI are composed of the trough-cross-stratified FA2 sandstones (e.g., logs 13–20 and logs 16–23 for bedset III and for bedsets IV–VI, respectively; Fig. 11B), passing into the heterolithic and muddier FA3 and FA4 downcurrent and towards the northwest (Fig. 11A). The scale of lateral accretion of these bedsets is such that it is revealed only by correlating beds across multiple logs. A case in point is that of bedsets V–VI in logs 16–22 (Fig. 11B), which show sigmoidal depositional profiles stacked in an overall eastward-accreting fashion.

To the east of log 23, the laterally accreted channel fills of Unit 1 passes rapidly into a few-meters-thick section (e.g., log 26; Fig. 11B) of FA6 overbank deposits, locally (bedsets VI–VII between logs 25 and 27; Fig. 11B) with interposed FA5 channel-margin deposits. It is worth noting that correlations in this channel–levee transition appear to slope westwards, suggesting that they accumulated in an inner-levee setting and thus west of a coeval levee crest.

Interpretation.--- The eastward-directed accreted organization of most of the channelized deposits of Unit 1, which is towards coeval levee deposits, suggests that they represent LAPs formed at the eastward accreted inner bank of a leveed channel. In light of northwards paleocurrent, the outcrops of Unit 1 can be thus seen as remnants of the deposits accumulated across a left-turning channel bend.

Unit 2

Unit 2 is relatively thin compared to other units, reaching a maximum thickness of c. 2 m (log 20, Fig. 11A), and can be differentiated from the deposits below being made dominantly of amalgamated sandstones (Fig. 11B–D). It was recognized principally in the Southwest Outcrop and in the North Outcrop, with a minor occurrence in the Southeast Outcrop.

Southwest Outcrop.--- In this outcrop, the unit begins with a basal erosion up to c. 2-m-deep (e.g., in log 64; Fig. 11D), across which an increase in grain size, mud-clast abundance, and degree of sandstone amalgamation is recorded in most logs (Fig. 11D). Unit 2 is bounded above by the basal

erosion of Unit 3, c. 2.5 m deep between logs 63 and 64 (Figs. 5B, 11D). What is preserved of Unit 2 at this location is composed chiefly of coarse-grained and mud-clast-rich FA1, in which basal scouring and sandstone bed amalgamation result in an overall disorganized cut-and-fill depositional character. North- northwest-wards. FA1 passes into less than 1 m of FA2 (Figs. 9D, 11D). Similar to the North Outcrop, FA1 is replaced eastwards by channel-margin deposits (FA5) and then by proximal overbank deposits (FA6) (in log 61 and log 60, respectively; Fig 11D).

North Outcrop.--- This outcrop, almost orthogonal to the north-northeast-directed mean paleocurrent (Fig. 2C), provides a c. 1-km-long cross section through Unit 2. As illustrated in Figure 11A, the large-scale cross-sectional shape of the unit is sigmoidal, with a topset in the southeast, overlying the outer-bank inner levee of Unit 1 (Fig. 11B). In north–south-oriented sections (e.g., logs 23–26, Fig. 11B), the top of the sigmoid appears flat, and the bedding is largely planar-parallel. Conversely, in east-west-oriented sections (e.g. logs 17–23, Fig. 11B), the top of the sigmoid dips gently towards the west and component beds thin proportionally both ways. A groove cast in log 22 indicates a north–south-oriented paleocurrent (Fig. 11A).

In the southeast (Figs. 9C, 11A), Unit 2 is composed mostly of mud-clast-rich amalgamated sandstones (FA1) and thins rapidly towards the east, translating into channel-margin (FA5) and proximal overbank deposits (FA6), most likely deposited in an inner-levee setting (Fig. 11B).

To the northwest of log 19, the uppermost part of the amalgamated sandstone becomes increasingly stratified, with FA1 partly replaced by trough cross-stratified FA2 sandstones (Fig. 10B). West-northwestward of log 13, the amalgamated sandstone thins further, pinching out past log 3C, and the upper part of the unit becomes increasingly mud-rich, being represented chiefly by FA3 between logs 11 and 4A, and FA4 between logs 3 and 3D.

Southeast Outcrop.--- The lowermost section of this outcrop, in logs 35–39 and farther south in logs 41–44 (Figs. 3A, C), comprises c. 1 meter of sandstone–mudstone (F5 and F6) couplets. Notably, the sandstone beds thin both towards the northeast and log 34 (Fig 3B), showing onlap terminations towards the north-northwest and log 35 (Fig 3A). The location of these deposits, which

is to the east and stratigraphically deeper than the inferred levee crest (Fig. 11A), suggests that they may represent proximal overbank deposits (FA6) stratigraphically equivalent with Unit 2.

Interpretation.--- Unit 2 is relatively coarser and its sandstones more amalgamated compared to Unit 1, which suggests deposition during a waxing phase of prevailing sediment discharge. Despite this, Unit 2 shows an architectural motif similar to that of the unit below, with channel-filling FAs transitioning into coeval inner-levee deposits at the easternmost end of the outcrop (Fig. 11A).

In the Southwest Outcrop, the FA composition suggests that deposition was dominantly in the most axial part of the channel, characterized by repeated cut-and-fill processes. In contrast, the shape and internal organization of Unit 2 in the North Outcrop, along with its position, i.e., overlying the outer-bank levee to the east, suggest its deposits are part of a bar attached to the outer bank, similar to large-scale examples documented from the subsurface by Nakajima et al. (2009) in sinuous channels in the upper slope of the Amazon Fan.

The FA6 deposits exposed in the Southeast Outcrop are interpreted to represent overbank deposits accumulated in the proximal and relatively steep part of the outer levee slope.

Unit 3

Reaching a thickness of up to c. 6 m (log 28, Fig. 12B), Unit 3 is the thickest unit of Complex 5. It is extensively exposed both in the Southwest Outcrop and in the North Outcrop (Fig 12A), and it comprises the lower section of the Southeast Outcrop. The base of Unit 3 is erosional in the Southwest Outcrop and slightly erosional in the North Outcrop, whereas its top surface is erosional in the Southeast Outcrop (logs 34–39; Fig. 12A), corresponding to the base of the channelized deposits of Unit 4.

Southwest Outcrop.--- In this outcrop, Unit 3 is composed dominantly of the amalgamated sandstones of FA1 and FA2. The trough-cross-stratified sandstones FA2 occur exclusively in northwestern localities, passing into coarser and more amalgamated sandstones (FA1) in the deeper part of the fill to the southeast (Figs. 12A, D). FA1 is characterized by a rather intricate cut-and-fill pattern suggestive of thalweg deposition, with frequent yet laterally discontinuous mud-breccia beds.

However, at the largest-scale, the boundaries of the few bedsets that could be tracked across the outcrop show an apparent dip towards the southwest, which may indicate a crude laterally accreted organization (Fig. 12D).

At the southeastern end of the outcrop, the channel-margin deposits of FA5 become widespread and transitions eastwards of log 60 (Fig. 12D) to proximal overbank deposits (FA6). It is worth noting that in the lower section of logs 60, FA5 sandwiches an up to 2-m-thick bedset, which comprises coarser and more amalgamated FA1 sandstones and extends laterally for several tens of meters (Fig. 12D, 14D). The position of this FA1 bedset, which is to the east of younger channel-margin deposits and to the west of the channel-levee transition, suggests that it may represent part of an outer-bank bar formed in an early stage of Unit 3 deposition.

North Outcrop.--- Stratigraphic variability in facies association composition of the North Outcrop allows subdividing Unit 3 into a lower and relatively sandier part and an upper part (Fig. 14C).

To the southeast, the lower part of Unit 3 begins with an alternation of the amalgamated sandstones of FA1 and FA2. Between logs 24 and 28, the top of this amalgamated sandstones is overlapped by younger beds (Fig. 14C), and their stratification appears to become steeper up-section (Fig. 12B), with apparent dips towards the north and the east away from log 27. These features suggest that the deposition of the lower part of Unit 3 at this location was able to build depositional relief. Towards the east-southeast (logs 30–31; Fig. 12B), the sandbody passes into a less amalgamated channel-margin deposit (FA5), which in turn evolves laterally into levee deposits in log 33 (Fig. 12B). Conversely, towards the north-northwest (starting from log 23; Fig. 12A), the amalgamated sandstones of FA1–FA2 are replaced by an alternation of the laterally accreted FA3, FA4, and subordinate FA2 (Figs. 9C, 10A, B, 14A). At log locality 5, FA3 bedsets show east-northeastward direction of accretion (Fig. 14A). A similar direction of accretion was observed in the FA2 bedsets occurring to the west of log locality 4A (Figs. 12A, 14B), which in log 3D records a groove cast with north–south orientation.

The upper part of Unit 3 is overall finer-grained compared to the lower part. To the southeast, it is composed of a few bedsets showing evidence of lateral accretion (Fig. 10B). One of these is well

exposed between log localities 27 and 29 (Fig. 14D), where an attempt to assess the direction of accretion was made with 35 bedding-orientation measurements. After removal of structural tilt, the accreted beds have a vector mean dip direction of c. 82° and dip angle of 3° (Fig. 15A), indicating average direction of accretion towards the east, which is at a high angle to the mean paleocurrent direction (Fig. 15B) recorded from sole casts (logs 31–33; Fig. 12A). These laterally accreted bedsets comprise variable proportions of FA2, FA3 and FA4 in their up-accretion dip part, passing into a toeset consisting of FA1 (Fig. 12B).

Similarly to the lower part, the upper part of Unit 3 becomes finer-grained and its sandstones less amalgamated towards the north-northwest, starting from log 27: the proportion of trough-cross-stratified sandstones (FA2) decreases rapidly in favor of the heterolithic FA3 and FA4 (Fig. 12A). Between logs 15 and 17, the direction of accretion of these deposits is offset by > 30° from the orientation of two groove casts, albeit varying within a broad range (Fig. 15C). In logs 3–3D, there is an increased proportions of FA2 and FA3, associated with an apparent direction of accretion towards the east and a north–south-oriented groove cast (Figs. 12A, 14B)

Southeast Outcrop.--- Recognition of Unit 3 in the Southeast Outcrop is based on depth relative to TBT1 and is thus debatable. The unit may correspond to less than c. 1 m of FA6 exposed in the lower section of logs 35–38 and logs 42–44, and to sandier deposits encountered in logs 39 and 41. At the latter log localities, the typical heterolithic deposits of FA6 is interspersed with a few lenticular sandstone bodies with erosional bases (the largest of which, exposed at log 41, is a few tens of meters wide and up to c. 2 m thick; Fig. 12A), which may represent the fills of crevasse channels.

Interpretation.--- Similar to the older Units 1-2, the channelized deposits of Unit 3 transition eastwards (e.g., log 60 in the Southwest Outcrop and log 30 in the North Outcrop) into a levee consisting of FA6. The apparent dip of correlated bedset boundaries in the Southwest Outcrop (Figs. 12D) suggests a crude lateral accretion towards the east, which is at a high angle to the mean paleocurrent direction and correlates to formation of eastward-directed LAPs in the North Outcrop, between logs 17–29 (Fig. 12B). Therefore, the deposits of Unit 3 can be interpreted as LAPs with variable degree of sandstone amalgamation and facies composition formed across the apex of a

left-turning bend. In keeping with this interpretation, FA6 exposed in the Southeast Outcrop might represent coeval overbank/crevasse-splay deposits accumulated to the west of the outer-bank levee crest.

Unit 4

This unit crops out extensively in the North Outcrop and in the Southeast Outcrop. In the Southwest Outcrop it is mostly cut away by modern erosion and/or covered by a thick soil (Fig. 13A), consisting of small exposures of overbank deposits to the west and channelized deposits to the east (e.g., in logs 66–67 and logs 63–60, respectively; Fig. 13A), which hereafter are not described further. The base of Unit 4 is locally erosional (i.e., in the Southeast Outcrop), whereas its top is gradational with the FA7 mudstones separating it from TBT1 (Fig. 13A).

Southeast Outcrop.--- The deposits of the Southeast Outcrop attributed to Unit 4 sit below several meters of FA7 mudstones separating them from TBT1 and above the FA6 proximal overbank deposits of Unit 3 (lower right corner of Fig. 11A). As such, the stratigraphic position of the unit is largely overlapping with that of the channelized part of Unit 3 to the west and the north (Figs. 3A–C).

Correlation of logs 35–37 highlight a channelized base, which is associated with an erosion a few metres deep in the southeast. Overall, the channel-filling deposits show southeastward-accreted organization (Fig. 13E). Down-accretion-dip, alternating FA3 and FA4 bedsets (log 35; Fig. 13D) pass into the coarser and amalgamated sandstones of FA2 and FA1 (logs 36–37; Fig. 13E), suggestive of near-thalweg deposition. A similar southeast-wards transition into coarser and amalgamated sandstones is observed between logs 39 and 41, which record a groove cast with northeast–southwest orientation (Fig. 13A). Farther towards the southeast, the abrupt change (i.e., logs 41–42; Fig. 13A) from the channelized FA1 to the proximal overbank deposits of FA6, provides a constraint for the parent channel pathway.

The upper section of the Southeast Outcrop consists of a c. 2-m-thick alternation of FA4, FA3, and subordinately FA2, in which cross-stratification and lateral accretion is widespread (e.g., logs 35–37; Fig. 13E).

North Outcrop.--- In this outcrop, Unit 4 is up to c. 4 m thick and spans a stratigraphic interval similar to that of the upper Southeast Outcrop (e.g., logs 34–37, Fig. 13A). The base of the unit is locally erosional, as suggested by two discrete erosional features up to c. 1 m deep and up to a few meters across in logs 26–29 (Figs. 14C, D). The scale of these features is similar to that the megaflutes documented by Elliott (2000a). However, the example of Figure 14C shows an orientation that is difficult to reconcile with mean paleocurrent orientation and is this best interpreted as which makes this erosional feature best interpreted as a sediment-failure scar.

The FA composition of Unit 4 in the North Outcrop is varied. To the east (logs 31–32, Fig. 13A), Unit 4 comprises FA2 in logs 31–33 and an association of FA3 and FA2 in logs 28A–30, capped by up to c. 2.5 meters of proximal overbank deposits (FA6). Conversely, northwest of log 27, the unit consists of FA6, which passes into distal overbank deposits (FA7) starting from log 17 (Fig.13A). Between log localities 23 and 28A, some of the FA6 sandstone beds can be seen to pinch out against the depositional relief of the unit below (Fig. 14C). In logs 10–4A (Figs 13A, C), several laterally discontinuous sandstone beds 10 to 50 cm thick are present in the FA7 mudstones, which suggest focusing of sand deposition in a low-lying area of the distal outer levee.

Interpretation.--- Spatial and stratigraphic distribution of the bulk of the channelized part of Unit 4 indicate that this unit records establishment of a new channel course, which was accompanied by axial erosion up to a few meters deep (Fig. 13A). To the west and the north, deposition was onto the pre-existing channel topography of Unit 3, which was locally remodelled, for example through formation of small features like those observed in the North Outcrop. These may represent erosional scours, or, alternatively, sediment failure scars affecting the channel bank.

Summary of Bar Deposits

Field observations indicate that the channelized facies associations of Complex 5 include a range of bars formed in various regions of the left-turning bend of a meandering, sinuous channel. To relate the documented bar deposits to specific regions of the channel bend, the occurrence of channel-fill vs. levee deposits and directional information (e.g., direction of accretion and paleocurrent from sole

casts) were used to map the likely channel pathway at the time of deposition of Units 1–4 (Fig. 16A–D). The inferred position of the thalweg is based on the occurrence of FA1, being the facies association characterized by the coarsest-grained and most amalgamated sandstones recognized in Complex 5 (Fig. 8). The resulting picture is one in which the Southwest Outcrop and the North Outcrop of Units 1–3 are upstream and downstream exposures of the deposits accumulated across a left-turning channel bend. Since very little is preserved of the channel fill of Unit 4, their deposits are not further described here.

Point Bar Deposits (LAPs)

LAPs make up the most of Unit 1 and Unit 3, suggesting point bars represent the dominant intra-channel architectural element of channel-levee Complex 5. Hereafter, LAPs will be described proceeding from the more upstream Southern Outcrop to the more downstream Northern Outcrop and from older to younger, paralleling them with similar deposits from the literature.

Upstream.--- Despite the amalgamated nature of the Southwest Outcrop, making it difficult to recognize lateral accretion locally, correlations and lateral trends in facies composition indicate that its channelized deposits were accumulated primarily by net southeastward lateral accretion of the inner bank, most likely in a location upstream of the bend apex (Fig. 16A–C).

The older LAPs (Unit 1) are composed of a lower sandy heterolithic deposit (FA3), intercalated with trough-cross-stratified sandstones (FA2), and an upper coarser-grained interval comprising locally amalgamated FA2 bedsets. Despite such stratigraphic variability in sandstone fraction, the facies composition of these LAPs indicates that deposition was from relatively fine-grained high- to low-concentration flows, similar to the suspension-dominated non-amalgamated to semi-amalgamated LAPs of Abreu et al. (2003).

By contrast, the younger LAPs of Unit 3 consist of amalgamated sandstone bedsets a few meters thick, defined by a crude, inclined stratification and passing into a more disorganized, coarse deposit with a cut-and-fill structure downaccretion dip. Bedset bases are erosional along most of their profile, implying that formation of LAPs was through discrete phases of enhanced lateral accretion and

degradation. Sandstones are more structured and less amalgamated up accretion dip, in what could be considered the middle set, becoming coarser-grained, richer in mud clasts and alternating with mud-clast breccias approaching the deepest part of the channel fill or the toeset. These LAPs show apparent lengths in the range 100–250 m, associated with stratigraphic distances between the up-dip end and the toeset of a few meters. The scale and facies composition of these amalgamated LAPs is similar to that of the mixed traction-suspension-dominated LAPs Abreu et al (2003) described in the Ross Formation of western Ireland (Elliott, 2000b) and show similarity with examples from the Rosario Formation of Baja California, Mexico (Dykstra and Kneller, 2009) and from the Isaac Formation of British Columbia, Canada (Arnott, 2007; Schwarz and Arnott, 2007).

Downstream.--- Due to a lesser degree of sandstone amalgamation, the scale of individual LAPs is best assessed in the North Outcrop. Insights into scale and facies composition of the older LAPs (Unit 1) are provided by bed-by-bed correlations in the accreted channel fills of bedsets V–VI of Unit 1 (Fig. 11B), which could be traced eastwards into coeval overbank deposits. The inclined stratification in these bedsets dips both ways from log 18 (Fig. 11B), suggesting that at this log locality the outcrop face is the closest to the northeastward-accreted inner bank of a left-turning bend (Fig. 16). The apparent length of the accreted deposit along the outcrop face (slightly oblique to direction of accretion) is c. 150 m, whereas inner-levee deposits first occur c. 190 m away from locality 18 (Fig. 11B). The stratigraphic distance between the top of the accreted deposit at locality 18 and correlative inner-levee deposits to the east (log 27) is c. 2 m. These observations imply that the meandering parent channel of Unit 1 was several tens of meters wide, with a bankfull depth more than c. 2 m. Facies composition and degree of sandstone amalgamation of these older LAPs indicate similarity with the suspension-dominated non-amalgamated LAPs of Abreu et al. (2003).

The younger LAPs (Unit 3) are particularly well exposed (Figs. 14C, D) in the southeast of the North Outcrop. Evidence of lateral accretion is the northeastward inclined stratification in the lower part of the unit, best expressed between logs 22 and 29 (Figs. 12B, 14C), and tilt-corrected measurements of bedding from the upper part of the unit, which indicate eastward accretion. This LAP reaches a maximum preserved thickness of c. 6 m in log locality 27, which was likely very close to the accreting inner bank of a left-turning channel bend.

The correlation transect between logs 27 and 30 provides a cross-sectional view slightly oblique to accretion direction of the upper part of Unit 3. This transect illustrates how the more elevated parts of the LAP (Figs. 12B, 14C, D), most likely encompassing their middle-set and part of the topset, are made of thinner-bedded, less amalgamated, and finer-grained sandstones (alternations of, in ascending order of abundance, FA5, FA3, and FA4), and are overall muddier. They pass down dip into amalgamated and mud-clast-rich sandstones (FA1) indicative of thalweg deposition at the toeset of a LAP (Figs. 12B, 14D). The preserved apparent length of each of the laterally accreted bedsets is the range 100–250 m (Fig. 12B), whereas the difference in elevation between the shallower and the deeper part of sigmoids imply bankfull depths in excess of a few meters. Therefore, thinning- and fining-upward progressions from coarse-grained and mud-clast rich amalgamated sandstones to alternations of more structured amalgamated sandstones and heterolithics like that characterizing log locality 27 (Fig. 14C) are the typical expression of lateral accretion.

All in all, the character of these younger LAPs is reminiscent of the mixed traction-suspension semi-amalgamated LAP type of Abreu et al. (2003), exemplified by Channel Complex Set 2 of the Solitary Channel (Tabernas Basin, Spain).

Inner- to Outer-Bank Transition Bar Deposits

The most striking aspect of the North Outcrop of Unit 3 is the downstream transition of the LAPs exposed in the southeast into the mud-rich heterolithic deposit that extends for over c. 500 m along-stream to the northwest of log 26 (Figs. 12A, 16C). This deposit consists of meter-thick alternations of FA3, FA4, and, subordinately, FA2 with an overall trough-cross-stratified organization, in which northeastward to eastward inclined stratification is widespread and generally at a high angle to paleocurrents (Fig. 15C). Despite its laterally accreted character, this heterolithic deposit appears way more mud-rich and thin-bedded than any other LAPs reported in the literature, with the most analogous being the suspension-dominated non-amalgamated LAP of Channel Complex Set 4 (Tabernas Basin, Spain) shown in Abreu et al. (2003). Its location, that is, downstream of correlative and sand-rich LAPs, is similar to that of inner-bank bars variously referred to as concave benches, oblique accretion deposits, or inner- to outer-bank transition bars (Straub et al., 2008; Straub et al.,

2011; Janocko et al., 2013b; Peakall and Sumner, 2015) and to that of fluvial counter bars (Smith et al., 2011).

Outer-Bank Bar Deposits

The occurrence of the amalgamated sandstone body that constitutes most of Unit 2 in the North Outcrop (Fig. 16B) may represent the expression of a bar formed at the outer bank, downstream of the bend apex and across the transition to the inner bank of the next bend. Exposed slightly oblique to mean paleocurrent, this deposit is characterized by a sigmoidal cross-sectional shape, defined by a flat base and a top surface dipping towards the west, with the topset leaning onto and transitioning into the outer-bank levee (Fig. 11A). Internally, the bedding thins proportionally towards both the topset and toeset, and facies composition is rather homogeneous, comprising medium- to coarse-grained amalgamated sandstones rich in mud clasts (FA1). These can be distinguished from those found in the toeset of the overlying LAPs of Unit 3 by being more stratified. It is worth noting that downstream of log 19 (Fig. 11A, B) and thus across the likely position of the inflection point (Fig. 16B), the amalgamated sandstone transitions into trough-cross-stratified sandstones (FA2), which in turn pass into a sandy heterolithic deposits (FA3) downstream of log 13 (Fig. 11A), indicating a significant change in depositional behaviour of flows.

Another possible outer-bank-bar deposit is that encountered in log 60, occurring sandwiched between the finer-grained channel-margin deposits (FA5) and immediately above outer-bank-levee deposits (Fig. 12D). Similar to the larger and better-preserved example exposed in the North Outcrop, this outer-bank bar is made of amalgamated beds of mud-clast-rich coarse sandstones (FA1). Based on the reconstructed pathway of the parent channel of Unit 3 (Fig. 16C), it can be speculated that this deposit were part of an up-apex outer-bank bar.

Other Laterally Accreted Deposits

The laterally accreted deposits lying between localities 3 and 3D in Unit 3 remain of ambiguous interpretation. These are represented by bedsets of, in decreasing order of abundance, FA2, FA3, and FA4 with east-ward direction of accretion (Figs. 12A and 14B). The coarser-grained character,

when compared to the correlative inner- to outer-bank transition bar deposits upstream, indicate they may represent the upstream tail of a coarser outer-bank bar. Laterally accreted and relatively mud-rich deposits from a similar location in a sinuous channel were observed in the subsurface (Jobe et al., 2015) and were produced in experimental deposits (Janocko et al., 2013b).

DISCUSSION

Stratigraphic Evolution of the investigated channel bend

Results indicate that the Southwest Outcrop and the North Outcrop span less than half a wavelength of the sinuosity of the parent channel of Units 1–3 at a left-turning bend (Fig. 16A–C) and that the Southeast Outcrop of Unit 4 records a later phase of channel-pathway reorganization (Fig. 16D). The idealized maps of Figure 16 indicate that throughout deposition of Units 1–3, the channel might have been moderately to highly sinuous (sinuosity > 1.2) and that the late phase of eastward switching was preceded by an increasingly sandier overbank deposition in the outer levee of Unit 1 and Unit 3 (Figs. 16B, C).

Sitting above the hemipelagic marlstones that separate it from Complex 4, the up to c. 4-m-thick Unit 1 (Fig. 11A), records the establishment of the parent channel of Complex 5 in the study area (Fig. 16A), most likely during a waxing phase of prevailing sediment discharge.

Correlations indicate that channel establishment was accompanied by an initial phase of levee growth. Only the inner part of the eastern outer bank levee is preserved, and the trajectory of sandstone-beds pinchouts suggests that the levee crest was a few hundreds of meters away from the channel margin and dominantly mud-rich (Figs. 11A, 16A). The lower section of the unit exposed in the easternmost log localities might represent part of the outer levee and is dominantly muddy too, signifying that at this stage very little sand escaped the channel (Fig. 11A). This early stage of muddy-levee growth appears to be quite common in the Tachrift System (Reguzzi et al., 2023; Zuffetti et al. 2023; Invernizzi et al., 2025, in this volume) but contrasts with classical models (Peakall et al., 2000; Kneller 2003). In fact, channel establishment of most systems is marked by an initial phase of incision (Schwarz and Arnott, 2007, Pyles et al., 2010, Morris et al., 2016; Bell et al., 2020). One possible

explanation for this initial phase of levee growth is that deposition was laterally confined by a pre-existing master levee. This question requires further investigation.

Unit 2 is sandier, and its sandstone more amalgamated, compared to Unit 1, indicating that its deposition marked a sudden increase of prevailing sediment discharge. The amalgamated sandstones exposed in the Southwest Outcrop show a rather disorganized cut-and-fill structure and correlate to an up to c. 2-m-thick amalgamated sandstone in the North Outcrop, interpreted to represent an outer-bank bar (Fig. 16B). In agreement with the available paleocurrent information, the channel pathway during deposition of Unit 2 was through the Southwest Outcrop and nearly parallel to most of the North Outcrop, which most likely extended between the outer bank and the inner bank of the bend downstream, straddling the inflection point. In the Southeast Outcrop, Unit 2 is exclusively represented by thin-bedded sandstone-mudstone couplets, representing the product of overbank sedimentation in an outer-levee setting (Fig. 16B).

Unit 3 is typified by larger and sandier LAPs compared to Unit 1, which show a marked along-stream variability in sedimentary facies association. In the Southwest Outcrop dominant accretion direction is towards the southeast and the high degree of sandstone amalgamation, coupled with a coarser grain-size, indicates that deposition occurred close to the bend apex (and potentially upstream of it; Fig. 16C), in an area occasionally subject to major erosion and reorganization. In the North Outcrop, accretion was towards the northeast in the lower part of the unit, and towards the east in the upper part of the unit, which entails that the initial bend sweep that brought the inner bank onto what was formerly the outer bank (i.e., the outer-bank bar of Unit 2) was followed by a phase of bend expansion and increase of sinuosity. The mapped channel pathway, constrained by directional data, suggests that the thalweg was to the north of the North Outcrop and that the more mud-rich and stratified deposits exposed to the east-northeast of log locality 25 were accumulating past the bend apex, over an extensive area straddling the inflection point. Therefore, these deposits may be the sedimentary expression of inner- to outer-bank transition bars (Janocko et al., 2013b), occurring in a position similar to that of fluvial counter bars (e.g., Smith et al., 2011). West of the inferred position of the outer-bank levee crest (i.e., in the Southeast Outcrop), the augmented amount of proximal overbank deposits, including small and relatively coarse crevasse-channel fills (Figs. 12A, 16C), witnesses

increased sand overbanking, which reflects incremental channel filling and reduction of the levee crest height (e.g., Khan and Arnott, 2011).

The generally poorly exposed Unit 4 marks switching of the channel to the east and erosion into older overbank deposits (Fig. 16D). The relocation of channel pathway recorded by Unit 4 might have been facilitated by a continuing reduction of the outer-bank levee crest height since deposition of Unit 2, as witnessed by the stratigraphic increase in sand overbanking observed in the Southeast Outcrop (Figs. 16B, C).

Stratigraphic and Along-Stream Changes in LAP Composition

Numerous examples of LAPs have been reported over the last two decades from both outcrop studies and interpretation of subsurface examples of sinuous slope channels (Elliott, 2000b; Abreu et al., 2003; Arnott, 2007; Wynn et al., 2007; Dykstra and Kneller, 2009; Kane et al., 2010; Janocko 2013a; Tek et al., 2021). Abreu et al. (2003) described three basic LAP types, namely amalgamated, semi-amalgamated, and non-amalgamated, which differ each from one another for facies composition reflecting the variable contribution of traction vs. suspension sedimentation to bank accretion. In contrast to amalgamated LAPs, which are typically dominated by relatively coarse or even pebbly massive sandstones, semi-amalgamated and non-amalgamated LAPs were defined as finer-grained and containing significant proportions of mud in their topsets (Abreu et al., 2003). Although these LAP types can be stratigraphically interleaved, suggesting that they might make lateral transition into one another (Abreu et al., 2003; Peakall and Sumner, 2015), along-stream variability of LAP character has hitherto not been documented at outcrop.

The results of detailed logging and correlation performed in this study suggest that the channelized deposits exposed in the Southwest Outcrop and in the southeast of the North Outcrop are upstream and downstream composites of the accreted inner bank of a leveed slope channel. The two outcrops are c. 500 meters away and differ in terms of facies association.

Results suggest that there is stratigraphic variability in the scale and facies composition of LAPs. For example, the LAPs developed in the early stage of deposition of Complex 5 (Unit 1) are

comparatively smaller and their sandstones less amalgamated than observed in Unit 3, lacking a mud-clast-rich coarse sandstone in their toesets. This suggests that prevailing sediment discharge plays a major role on processes governing LAP formation and that different LAP types may alternate in the stratigraphy or stack following predictable patterns as result of changes in sediment input across a range of temporal scales.

The best-exposed Unit 3 illustrates how LAPs of scale and composition similar to amalgamated examples from literature (e.g., Abreu et al., 2003; Arnott, 2007; Schwarz and Arnott, 2007; Dykstra and Kneller, 2009) can make downstream transition into less-amalgamated and finer-grained LAPs (semi-amalgamated, mixed traction-suspension- and suspension-dominated LAP types of Abreu et al., 2003) over distances of a few hundreds of meters. This transition is associated with a considerable change in facies and lithological association (Fig. 17A), being the downstream and less-amalgamated LAPs more layered with intervening mudstones up to a few tens of cm thick over most of their along-dip profile. The upstream LAPs are thought to have formed very close to or even slightly upstream of the bend apex, in an area of the inner bank occasionally subject to major erosion, whereas, as shown in the following discussion, the less amalgamated composite is past the apex and transitional to a laterally extensive area of flow separation. In a companion article in this volume, Pantopoulos et al. (2025) present a detailed quantification of the internal heterogeneity of these LAPs, which can be applied for static reservoir modelling.

Linking LAPs and inner- to outer-bank transition bars

In the North Outcrop of Unit 3, LAPs were observed to make rapid transition from a traction-suspension semi-amalgamated type (Abreu et al., 2003) to a remarkably more mud-rich, heterolithic deposit, which extends with little facies changes over a length of c. 500 metres and most likely spans the inflection point (Figs. 16C, 17B). This deposit shows some similarity with the relatively fine-grained suspension-dominated non-amalgamated LAPs of Abreu et al. (2003), which were hypothesized to form in low-velocity separation zones developed downstream of bend apices. The occurrence of these deposits was predicted by laboratory and numerical modelling (Straub et al., 2008, 2011; Janocko et al., 2013b; see also Peakall and Sumner, 2015) and documented by seismic

interpretation of subsurface analogues (e.g., Babonneau et al. 2010). However, Peakall and Sumner (2015) noted that these fine-grained deposits, variously referred to as concave benches (Straub et al., 2008), oblique-accretion deposits (Straub et al., 2011), or inner- to outer-bank transition bars (Janocko et al., 2013b), occur when LAPs are missing or are superimposed onto LAPs and might thus be genetically and temporally underlated to point bars. Results of this study contrast with the observation of Peakall and Sumner (2015) in that they document that LAPs and mud-rich heterolithic bar deposits accumulated downstream can be contemporaneous sedimentary products. Since the processes governing deposition in the flow-separation zone are arguably different from those shaping the inner bank upstream (Straub et al., 2008; Straub et al., 2011; Janocko et al., 2013b), it is suggested that the use of LAP to refer to inner- to outer-bank transition bar deposits (e.g., Abreu et al., 2003) should be avoided. Analogously to the use of the term *point bar* in turbidite-channel studies, it is proposed that similar laterally accreted deposits accumulated in the inner- to outer-bank transition are referred to as turbidite counter-bar deposits.

First Outcrop Documentation of Outer-Bank Bars

Outer-bank bars were first documented through seismic imaging in a sinuous paleochannel of the Amazon fan by Nakajima et al. (2009), who described them as relatively thick (up to 150 meters) and extensive (c. 1.5 kilometers wide) bars attached to the outer bank and characterized by continuous internal reflectors dipping towards the thalweg. There is general agreement in interpreting them as the result of enhanced deposition on the outsides of bends as flows lose their capacity when running up the outer bank (Straub et al., 2008, 2011; Nakajima et al., 2009; Janocko et al., 2013b; Peakall and Sumner, 2015), although some authors have suggested that other factors are required for their formation, e.g., an outward-directed flow helicoid; Janocko et al. (2013b). Experimental results predicted that outer-bank bars might have coarser composition compared to coeval LAPs (Straub et al., 2008, 2011), but no direct lithological observation from cores or outcrop is available to confirm this.

Despite of a scale two orders of magnitude smaller than the seismically imaged outer-bank bars of Nakajima et al. (2009), the example from the North Outcrop of Unit 2 shows a similar occurrence

and cross-sectional shape. It leans onto the outer bank downstream of the bend apex, extending beyond the inferred position of the inflection point (Fig. 16B), and is characterized by a sigmoidal profile with a top dipping towards the contemporaneous thalweg. This down-apex outer-bank bar deposit consists of an amalgamated sandstone bedset up to c. 2 m thick and more than c. 600 m wide alongstream with a rather homogenous facies composition, dominated by mud-clast-rich coarse sandstone (Fig. 17C). These sandstones are texturally similar to those making the toesets of the stratigraphically associated LAPs, from which, however, they can be distinguished for being better stratified. Downcurrent, this small-scale example of an outer-bank bar transitions laterally into a more stratified sandstone, and then into sandy heterolithics (see also Pantopoulos et al., 2025, this volume), suggesting a significant along-stream change in flow conditions across the inflection point. The other minor occurrence of outer-bank bar deposits documented in the Southeast Outcrop of Unit 3 indicates that accretion of coarse-grained deposit at the outer bank can extend upstream of the bend apex.

It is argued that longer-lived and thus larger and more composite outer-bank bars could show a significantly more complex internal structure, resulting from variations in prevailing sediment discharge, adjustments of the channel morphology or a combination thereof.

CONCLUSIONS

Detailed logging and correlation of fifty-nine stratigraphic logs allowed detailed analysis of the stratigraphy and facies composition of the c. 20-m-thick main sandstone body of the turbidite channel–levee Complex 5 (Tachrift System, Late Tortonian of NE Morocco). Logs were measured across three main outcrops with various orientations relative to the north-directed mean paleocurrent, which provides an unprecedented three-dimensional view of channel-fill sedimentary architecture. Supported by stratigraphic correlations and directional data, the distribution of facies and facies associations indicates that the dataset spans over approximately one-half wavelength of sinuosity of the parent channel, sampling the fill of a left-turning bend and part of the related outer-bank levee. Four stratigraphic units were recognized, which record establishment and levee development (Unit 1), aggradation and inner-bend translation (Units 2–3), and switching (Unit 4) of

a moderately to highly sinuous meandering channel. As a result, lateral-accretion packages (LAPs) that accumulated at the inner bank represent the main channel-filling element, locally accompanied by sand-rich deposits accumulated at the outer bank.

The largest and best-exposed examples of LAPs (in Unit 3) were described in detail from two outcrops that are 500 m apart alongstream, documenting a considerable change in degree of sandstone amalgamation and facies-association composition, interpreted to reflect their different position across the bend apex. The LAPs of the upstream outcrop internally show several erosional surfaces suggesting frequent reactivation of the inner bank as if the flow was impinging at a high angle onto the bank upstream of the bend apex. By contrast, the LAPs downstream of the bend apex comprises finer-grained and less amalgamated sandstones, which pass into an alternation of sandstone and mudstone beds up the accretion dip. Farther downstream, these LAPs transition into a largely mud-rich heterolithic deposit characterized by inclined stratification and with accretionary geometries with dips at a high angle to the paleocurrent and toward the inferred position of the thalweg. This deposit is interpreted as the product of suspension deposition in a flow-separation zone straddling the inflection point and can be regarded as the expression of turbidite counter-bars, similar to fluvial counter-bars.

This work provide insights into downstream sedimentary heterogeneity of LAPs and documents outer-bank bar deposits and turbidite counter-bar deposits for the first time from outcrops.

Acknowledgments

We thank the Turbidite Research Group for financial support, with funding provided by AkerBP, CNOOC, ConocoPhillips, ENI, Harbour Energy, Murphy, OMV, PetroChina and OXY, and Prof. Hassan Tabyaoui for logistical support. The local Authorities of Douar Tachrift and Ras El Ksar are thanked for providing access to outcrops. We also wish to thank the Hachimi family at Ait El Baji for their invaluable help and warm hospitality.

References

- Abreu, V., Sullivan, M., Pirmez, C., and Mohrig, D., 2003, Lateral accretion packages (LAPs): an important reservoir element in deep water sinuous channels: *Marine and Petroleum Geology*, v. 20, p. 631-648.
- Arnott, R.W.C., 2007, Stratal architecture and origin of lateral accretion deposits (LADs) and conterminous inner-bank levee deposits in a base-of-slope sinuous channel, lower Isaac Formation (Neoproterozoic), East-Central British Columbia, Canada: *Marine and Petroleum Geology*, v. 24, p. 515-528.
- Arnott, R.W.C., Tilston, M., Fraino, P., Navarro, L., Dumouchel, G., and Miklovich, N., 2021. Laterally accreting sinuous channels and their deposits: The Goldilocks of deep-water slope systems: *Journal of Sedimentary Research*, v. 91, p. 451-463.
- Babonneau, N., Savoye, B., Cremer, M., Bez, M., 2010, Sedimentary architecture in meanders of a submarine channel: detailed study of the present Congo turbidite channel (Zaiango Project): *Journal of Sedimentary Research*, v. 80, p. 852–866.
- Benzaquen, M., 1965, Etude stratigraphique préliminaire des formations du bassin de Guercif. Direct: Mines et Géologie, Service de la Cartographie Géologique, Bureau d'études des bassins Sédimentaires, 73 p.
- Bernini, M., Boccaletti, M., El Mokhtari, J., Gelati, R., Moratti, G., and Papani, G., 1994, Geologic-structural Map of the Taza–Guercif Neogene basin (North-eastern Morocco). Scale 1: 50.000. Società Elaborazioni Cartografiche, Firenze.
- Bernini, M., Boccaletti, M., Gelati, R., Moratti, G., Papani, G., and Mokhtari, J.E., 1999, Tectonics and sedimentation in the Taza-Guercif Basin, Northern Morocco: Implications for the Neogene Evolution of the Rif-Middle Atlas Orogenic system: *Journal of Petroleum Geology*, v. 22, p. 115-128.
- Bernini, M., Boccaletti, M., Moratti, G., and Papani, G., 2000, Structural development of the Taza-Guercif Basin as a constraint for the Middle Atlas Shear Zone tectonic evolution: *Marine and Petroleum Geology*, v. 17, p. 391-408.

Bouma, A.H., 1962. *Sedimentology of Some Flysch Deposits. A Graphic Approach to Facies Interpretation*. Elsevier Publishing Company, p. 168.

Bell, D., Hodgson, D.M., Pontén, A.S., Hansen, L.A., Flint, S.S., and Kane, I.A., 2020, Stratigraphic hierarchy and three-dimensional evolution of an exhumed submarine slope channel system: *Sedimentology*, v. 67, p. 3259-3289.

Capella, W., Hernandez-Molina, F.J., Flecker, R., Hilgen, F.J., Hssain, M., Kouwenhoven, T.J., van Oorschot, M., Sierro, F.J., Stow, D., Trabucho-Alexandre, J., Tulbure, M.A., de Weger, W., Yousfi, M.Z., and Krijgsman, W., 2017, Sandy contourite drift in the late Miocene Rifian Corridor (Morocco): Reconstruction of depositional environments in a foreland-basin seaway: *Sedimentary Geology*, v. 355, p. 31–57.

Capella, W., Barhoun, N., Flecker, R., Hilgen, F.J., Kouwenhoven, T., Matenco, L.C., Sierro, F.J., Tulbure, M.A., Yousfi, M.Z., and Krijgsman, W., 2018, Palaeogeographic evolution of the late Miocene Rifian Corridor (Morocco): reconstructions from surface and subsurface data: *Earth Science Reviews*, v. 180, p. 37–59.

Capella, W., Flecker, R., Hernández-Molina, F.J., Simon, D., Meijer, P.T., Rogerson, M., Sierro, F.J., and Krijgsman, W., 2019, Mediterranean isolation preconditioning the Earth System for late Miocene climate cooling: *Scientific Reports*, v. 9, no. 3795.

Cronin, B.T., Hurst, A., Celik, H., and Türkmen, I., 2000, Superb exposure of a channel, levee and overbank complex in an ancient deep-water slope environment: *Sedimentary Geology*, v. 132, p. 205-216.

Das, H.S., Imran, J., Pirmez, C., and Mohrig, D., 2004, Numerical modeling of flow and bed evolution in meandering submarine channels: *Journal of Geophysical Research: Oceans*, v. 109, no. C10.

de Lamotte, D.F., Leturmy, P., Missenard, Y., Khomsi, S., Ruiz, G., Saddiqi, O., Guillocheau, F., and Michard, A., 2009, Mesozoic and Cenozoic vertical movements in the Atlas system (Algeria, Morocco, Tunisia): an overview: *Tectonophysics*, v. 475, p. 9-28.

De Weger, W., Hernández-Molina, F.J., Miguez-Salas, O., De Castro, S., Bruno, M., Chiarella, D., Siirro, F.J., Blackbourn, G., and Manar, M.A., 2021, Contourite depositional system after the exit of a strait: Case study from the late Miocene South Rifian Corridor, Morocco: *Sedimentology*, v. 68, p. 2996-3032.

Dykstra, M., and Kneller, B., 2009. Lateral accretion in a deep-marine channel complex: implications for channelized flow processes in turbidity currents: *Sedimentology*, v. 56, p. 1411–1432.

Elliott, T., 2000a, Megaflute erosion surfaces and the initiation of turbidite channels: *Geology*, v. 28, p. 119-122.

Elliott, T., 2000b, Depositional architecture of a sand-rich, channelized turbidite system: the upper carboniferous Ross sandstone formation, western Ireland, *in* Slatt, R.M., Coleman, J., Rosen, N.C., Nelson, H., Bouma, A.H., Styzen, M.J. and Lawrence, D.T., eds., *Deep-Water Reservoirs of the World: Gulf Coast Section Society for Sedimentary Geology, GCSSEPM Foundation Annual Bob F. Perkins Research Conference Proceedings*, v. 20, p. 342–373.

El Kati, I., Benammi, M., Tabyaoui, H., Ouabid, M., and Benammi, M., 2022, Structural style and deformation mechanism of Neogene series of the Guercif basin (NE-Morocco): *Journal of Iberian Geology*, v. 48, p. 281-296.

Felletti, F., Marini, M., El Kati, I. and Tabyaoui, H., 2020, The Tachrift channel-levée turbidite complexes (Tortonian) of the Taza-Guercif basin (South Rifian Corridor, NE Morocco): *Journal of Maps*, v. 16, p. 902-917.

Felletti, F., Pantopoulos, G., Zuffetti, C., Reguzzi, S., Invernizzi, D., Bellin, N., Marini, M., El Kati, I., Savi, E., Tabyaoui, H. and McArthur, A., 2023, The Tachrift Project: sedimentary architecture of turbidite channel-levée deposits (Tachrift Turbidite System, Taza-Guercif Basin, Tortonian, NE Morocco): *Rendiconti Online della Società Geologica Italiana*, v. 59, p. 80-88.

Flecker, R., Krijgsman, W., Capella, W., de Castro Martins, C., Dmitrieva, E., Mayser, J.P., Marzocchi, A., Modestou, S., Ochoa, D., Simon, D., Tulbure, M., van den Berg, B., van der Schee, M., de Lange, G., Ellam, R., Govers, R., Gutjahr, M., Hilgen, F., Kouwenhoven, T., Lofi, J., Meijer,

P., Sierro, F.J., Bachiri, N., Barhoun, N., Alami, A.C., Chacon, B., Flores, J.A., Gregory, J., Howard, J., Lunt, D., Ochoa, M., Pancost, R., Vincent, S., and Yousfi, M.Z., 2015, Evolution of the Late Miocene Mediterranean-Atlantic gateways and their impact on regional and global environmental change: *Earth-Science Reviews*, v. 150, p. 365–392.

Fukuda, S., de Vet, M.G.W., Skevington, E.W.G., Bastianon, E., Fernández, R., Wu, X., McCaffrey, W.D., Naruse, H., Parsons, D. R. and Dorrell, R. M, 2023, Inadequacy of fluvial energetics for describing gravity current autosuspension: *Nature Communications*, v. 14, no. 2288.

Gelati, R., Moratti, G., and Papani, G., 2000, The Late Cenozoic sedimentary succession of the Taza-Guercif Basin, South Rifian Corridor, Morocco: *Marine and Petroleum Geology*, v. 17, p. 373–390.

Hafid, M., Zizi, M., Bally, A.W., and Salem, A.A., 2006, Structural styles of the western onshore and offshore termination of the High Atlas, Morocco: *Comptes Rendus Geoscience*, v. 338, p. 50-64.

Invenizzi, D., Pizzutto, M., Felletti, F., Pantopoulos, G., Marini, M., and McArthur, A., 2025, Reconstruction of the sedimentary heterogeneity in outcropping deep-water channel levee deposits (Taza-Guercif Basin, late Tortonian, NE Morocco): *Journal Sedimentary Research*. THIS VOLUME/ISSUE

Janbu, N.E., Nemeč, W., Kirman, E., and özaksoy, V., 2007, Facies Anatomy of a Sand-Rich Channelized Turbiditic System: The Eocene Kusuri Formation in the Sinop Basin, North-Central Turkey, *in* Nichols, G. Paola, C. Williams, E.A., eds, *Sedimentary Processes, Environments and Basins: A Tribute to Peter Friend*, International Association of Sedimentologists, Special Publication 38, p. 457-517.

Janocko, M., Nemeč, W., Henriksen, S., and Warchoł, M., 2013a, The diversity of deep-water sinuous channel belts and slope valley-fill complexes: *Marine and Petroleum Geology*, v. 41, p. 7-34.

Janocko, M., Cartigny, M.B.J., Nemeč, W., and Hansen, E.W.M., 2013b, Turbidity current hydraulics

and sediment deposition in erodible sinuous channels: laboratory experiments and numerical simulations: *Marine and Petroleum Geology*, v. 41, p. 222–249.

Jobe, Z.R., Sylvester, Z., Parker, A.O., Howes, N., Slowey, N., and Pirmez, C., 2015, Rapid adjustment of submarine channel architecture to changes in sediment supply: *Journal of Sedimentary Research*, v. 85, p. 729-753.

Jobe, Z.R., Howes, N.C., and Auchter, N.C., 2016, Comparing submarine and fluvial channel kinematics: Implications for stratigraphic architecture: *Geology*, v. 44, p. 931-934.

Jobe, Z. R., Howes, N.C., Straub, K. M., Cai, D., Deng, H., Laugier, F.J., Pettinga, L.A., and Shumaker, L. E., 2020, Comparing Aggradation, Superelevation, and Avulsion Frequency of Submarine and Fluvial Channels: *Frontiers in Earth Science*, v. 8, no. 53.

Kane, I.A., and Hodgson, D.M., 2011, Sedimentological criteria to differentiate submarine channel levee subenvironments: exhumed examples from the Rosario Fm. (Upper Cretaceous) of Baja California, Mexico, and the Fort Brown Fm.(Permian), Karoo basin, S. Africa: *Marine and Petroleum Geology*, v. 28, p. 807-823.

Kane, I.A., Catterall, V., McCaffrey, W.D., and Martinsen, O. J., 2010, Submarine channel response to intrabasinal tectonics: The influence of lateral tilt: *American Association of Petroleum Geologists, Bulletin*, v. 94, p. 189-219.

Keevil, G.M., Peakall, J., Best, J.L., and Amos, K.J., 2006, Flow structure in sinuous submarine channels: Velocity and turbulence structure of an experimental submarine channel: *Marine Geology*, v. 229, p. 241-257.

Khan, Z.A., and Arnott, R.W.C., 2011, Stratal attributes and evolution of asymmetric inner- and outer-bend levee deposits associated with an ancient deep-water channel-levee complex within the Isaac Formation, southern Canada: *Marine and Petroleum Geology*, p. 28, p. 824-842.

Kneller, B., 2003. The influence of flow parameters on turbidite slope channel architecture: *Marine and Petroleum Geology*, v. 20, p. 901-910.

Krijgsman, W., and Langereis, C.G. 2000, Magnetostratigraphy of the Zobzit and Koudiat Zarga sections (Taza-Guercif basin, Morocco): implications for the evolution of the Rifian Corridor: *Marine and Petroleum Geology*, v. 17, p. 359-371.

Krijgsman, W., Langereis, C.G., Zachariasse, W.J., Boccaletti, M., Moratti, G., Gelati, R., Iaccarino, S., Papani, G., and Villa, G., 1999, Late Neogene evolution of the Taza–Guercif Basin (Rifian Corridor, Morocco) and implications for the Messinian salinity crisis: *Marine Geology*, v. 153, p. 147-160.

Lowe, D.R., 1982, Sediment gravity flows; II, Depositional models with special reference to the deposits of high-density turbidity currents: *Journal of Sedimentary Petrology*, v. 52, p. 279-297.

McHargue, T., Pyrcz, M.J., Sullivan, M.D., Clark, J.D., Fildani, A., Romans, B.W., Covault, J.A., Levy, M., Posamentier, H.W., and Drinkwater, N.J., 2011, Architecture of turbidite channel systems on the continental slope: Patterns and predictions: *Marine and Petroleum Geology*, v. 28, p. 728–743.

Menard, H.W., 1955, Deep-sea channels, topography, and sedimentation: *American Association of Petroleum Geologists, Bulletin*, v. 39, p. 236–255.

Morris, E.A., Hodgson, D.M., Flint, S., Brunt, R. L., Luthi, S. M., and Kolenberg, Y., 2016, Integrating outcrop and subsurface data to assess the temporal evolution of a submarine channel-levee system: *American Association of Petroleum Geologists, Bulletin*, v. 100, p. 1663-1691.

Mutti, E., 1992, *Turbidite Sandstones*: AGIP, Istituto di Geologia, Università di Parma, 275 p.

Mutti, E., and Normark, W. R., 1987, Comparing examples of modern and ancient turbidite systems: problems and concepts, *in* Leggett, J.K., and Zuffa, G.G., eds., *Marine clastic Sedimentology: Concepts and Case Studies*: London, Graham and Trotman, p. 1-38.

Mutti, E., and Normark, W.R., 1991, An integrated approach to the study of turbidite systems, *in* Weimer, P., and Link, M., eds., *Seismic Facies and Sedimentary Processes of Submarine Fans and Turbidite Systems*: Springer-Verlag, p. 75–106.

- Nakajima, T., Peakall, J., McCaffrey, W.D., Paton, D.A., and Thompson, P.J., 2009, Outer-bank bars: a new intra-channel architectural element within sinuous submarine slope channels: *Journal of Sedimentary Research*, v. 79, p. 872–886.
- Ogg, J.G., 2020, Geomagnetic Polarity Time Scale, *in* Gradstein, F.M., Ogg, J.G., Schmitz, M.D., Ogg, G.M., eds., *Geologic Time Scale 2020*: Elsevier, p. 159-192.
- Pantopoulos, G., Marini, M., Invernizzi, D., El Kati, I., D. McArthur, A., Felletti, F., 2025, Quantification of the internal heterogeneity across a submarine channel bend: a unique example from the late Tortonian Tachrift channel complex 5 (Taza-Guercif Basin, NE Morocco): *Journal Sedimentary Research*. THIS VOLUME/ISSUE
- Patacci, M., 2016, A high-precision Jacob's staff with improved spatial accuracy and laser sighting capability: *Sedimentary Geology*, v. 335, p. 66-69.
- Peakall, J., and Sumner, E.J., 2015, Submarine channel flow processes and deposits: A process-product perspective: *Geomorphology*, v. 244, p. 95-120.
- Peakall, J., McCaffrey, B., and Kneller, B., 2000, A process model for the evolution, morphology, and architecture of sinuous submarine channels: *Journal of Sedimentary Research*, v. 70, p. 434-448.
- Peakall, J., Amos, K.J., Keevil, G.M., Bradbury, P.W., and Gupta, S., 2007, Flow processes and sedimentation in submarine channel bends: *Marine and Petroleum Geology*, v. 24, p. 470-486.
- Phillips, S., 1987, Dipmeter interpretation of turbidite-channel reservoir sandstones, Indian Draw Field, New Mexico, *in* Tillman, R.W., and Weber, K.J., eds., *Reservoir Sedimentology*: SEPM, Special Publication 40, p. 113–128.
- Pratt, J.R., Barbeau, D.L.Jr., Izykowski, T.M., Garver, J.I., and Emran, A., 2016, Sedimentary provenance of the Taza-Guercif basin, south Rifian Corridor, Morocco: Implications for basin emergence: *Geosphere*, v. 12, p. 221-236.

Pyles, D.R., Jennette, D.C., Tomasso, M., Beaubouef, R.T., and Rossen, C., 2010, Concepts learned from a 3D outcrop of a sinuous slope channel complex: Beacon Channel Complex, Brushy Canyon Formation, West Texas, USA: *Journal of Sedimentary Research*, v. 80, p. 67-96.

Reguzzi, S., Marini, M., Felletti, F., El Kati, I., Zuffetti, C., and Tabyaoui, H., 2023, Stratigraphic evolution of a spectacularly exposed turbidite channel belt from the Tachrift System (late Tortonian, north-East Morocco) : *Sedimentology*, v. 70, p. 1075-1109.

Reimchen, A.P., Hubbard, S.M., Stright, L., and Romans, B.W., 2016, Using sea-floor morphometrics to constrain stratigraphic models of sinuous submarine channel systems: *Marine and Petroleum Geology*, v. 77, p. 92-115.

Sani, F., Zizi, M., and Bally, A.W., 2000, The Neogene–Quaternary evolution of the Guercif Basin (Morocco) reconstructed from seismic line interpretation: *Marine and Petroleum Geology*, v. 17, p. 343-357.

Schwarz, E., and Arnott, R.W.C., 2007, Anatomy and evolution of a slope channel-complex set (Neoproterozoic Isaac Formation, Windermere Supergroup, southern Canadian Cordillera): implications for reservoir characterization: *Journal of Sedimentary Research*, v. 77, p. 89-109.

Smith, D.G., Hubbard, S.M., Lavigne, J.R., Leckie, D.A. and Fustic, M., 2011, Stratigraphy of counter-point-bar and eddy-accretion deposits in low-energy meander belts of the Peace-Athabasca Delta, northeast Alberta, Canada, *in* Davison, S., and North, C., eds., *From River To Rock Record: The Preservation Of Fluvial Sediments And Their Subsequent Interpretation: SEPM Special Publication 97*, p. 143–152.

Sprague, A.R.G., Garfield, T.R., Goulding, F.J., Beaubouef, R.T., Sullivan, M.D., Rossen, C., Champion, K.M., Sickafoose, D.K., Abreu, V., Schellpeper, M.E., Jensen, G.N., Jennette, D.C., Pirmez, C., Dixon, B.T., Ying, D., Ardill, J., Mohrig, D.C., Porter, M.L., Farrell, M. E., and Mellere, D., 2005, Integrated slope channel depositional models: the key to successful prediction of reservoir presence and quality in offshore west Africa: Veracruz, Mexico, Colegio de Ingenieros Petroleros de Mexico, Cuarto EExitep, p. 1–13.

Straub, K.M., Mohrig, D., McElroy, B., and Buttles, J., 2008, Interactions between turbidity currents and topography in aggrading sinuous submarine channels: a laboratory study. *Geological Society of America, Bulletin*, v. 120, p. 368–385.

Straub, K.M., Mohrig, D., Buttles, J., McElroy, B., and Pirmez, C., 2011, Quantifying the influence of channel sinuosity on the depositional mechanics of channelized turbidity currents: a laboratory study: *Marine and Petroleum Geology*, v. 28, p. 744–760.

Taylor, A.M., and Goldring, R., 1993. Description and analysis of bioturbation and ichnofabric: *Geological Society of London Journal*, v. 150, p. 141-148.

Tek, D.E., McArthur, A.D., Poyatos-Moré, M., Colombera, L., Patacci, M., Craven, B., and McCaffrey, W. D., 2021, Relating seafloor geomorphology to subsurface architecture: How mass-transport deposits and knickpoint-zones build the stratigraphy of the deep-water Hikurangi Channel: *Sedimentology*, v. 68, p. 3141-3190.

Timbrell, G., 1993, Sandstone architecture of the Balder Formation depositional system, UK Quadrant 9 and adjacent areas, *in* Parker, J.R. ed., *Petroleum Geology of Northwest Europe: Proceedings of the 4th Conference*, Geological Society of London, p. 107–121.

Wells, M.G., and Dorrell, R.M., 2021, Turbulence Processes within Turbidity Currents: *Annual Review of Fluid Mechanics*, v. 53, p. 59-83.

Wynn, R.B., Cronin, B.T., and Peakall, J., 2007, Sinuous deep-water channels: Genesis, geometry and architecture: *Marine and Petroleum Geology*, v. 24, p. 341-387.

Zuffetti, C., Felletti, F., and Marini, M., 2023, Turbidite channel-levée transitions: insights from the Tachrift system (Complex 6, Taza-Guercif Basin, NE Morocco): *Rendiconti Online della Società Geologica Italiana*, v. 59, p. 21-27.

CAPTIONS

hand side) (modified, after Krijgsman et al., 1999). Numbers 1–9 identify the channel–levee complexes of Felletti et al. (2020). Magnetochron nomenclature and age after Ogg (2020).

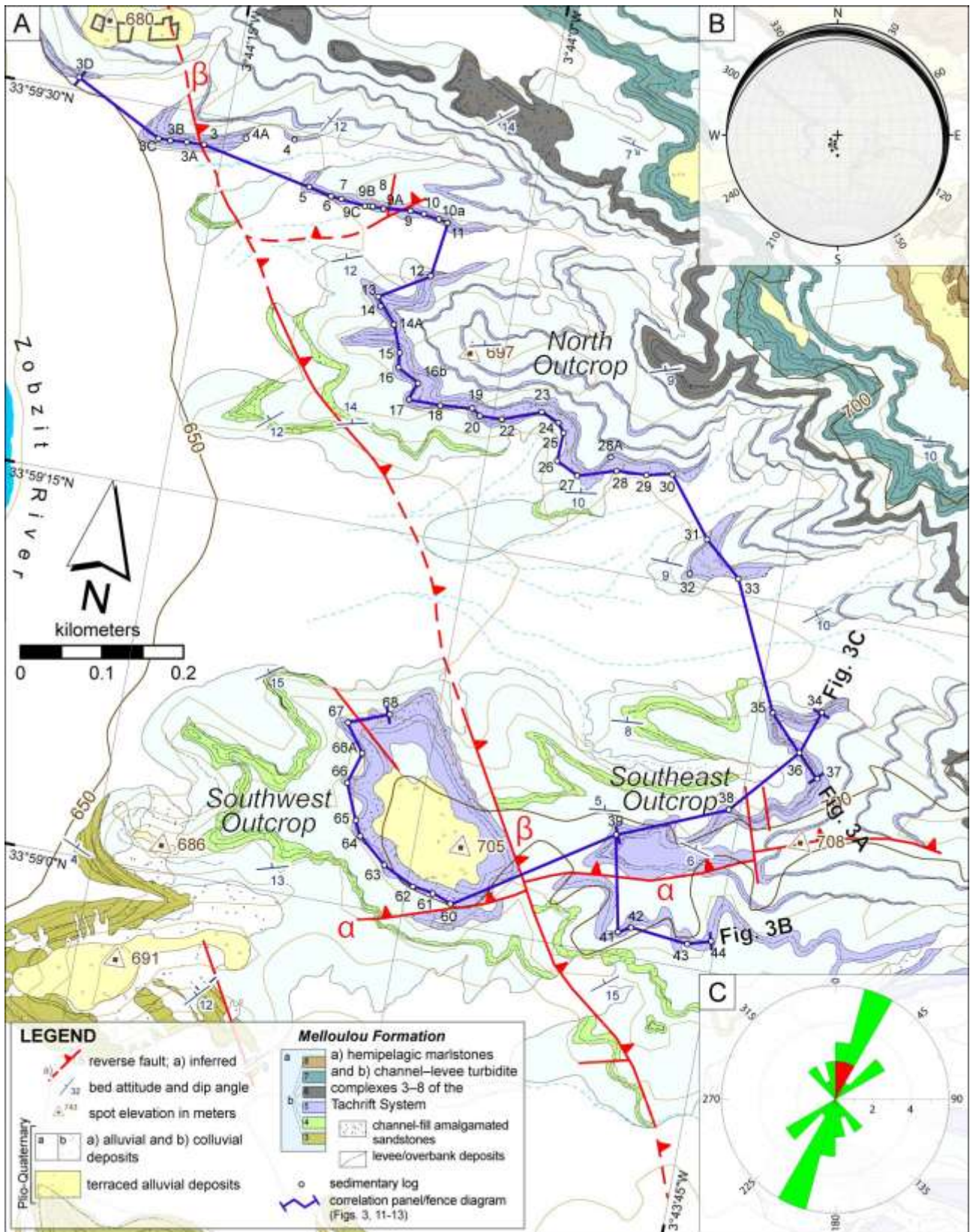


Fig. 2. A) Geological map (modified, after Felletti et al., 2020) with location of sedimentary logs and correlation panels. The Greek letters α and β identify the faults discussed in the text. B) Equal-area stereonet plot (lower-hemisphere projection) of bedding attitudes. Dots (with mean dip direction and dip angles) are poles to bedding planes measured in the lower part of the investigated stratigraphy. C) Paleocurrent information for the main sandstone body of channel–levee Complex 5. The equal-area rose diagram shows the orientation of 18 groove casts (green) and the direction of four flute casts (red).

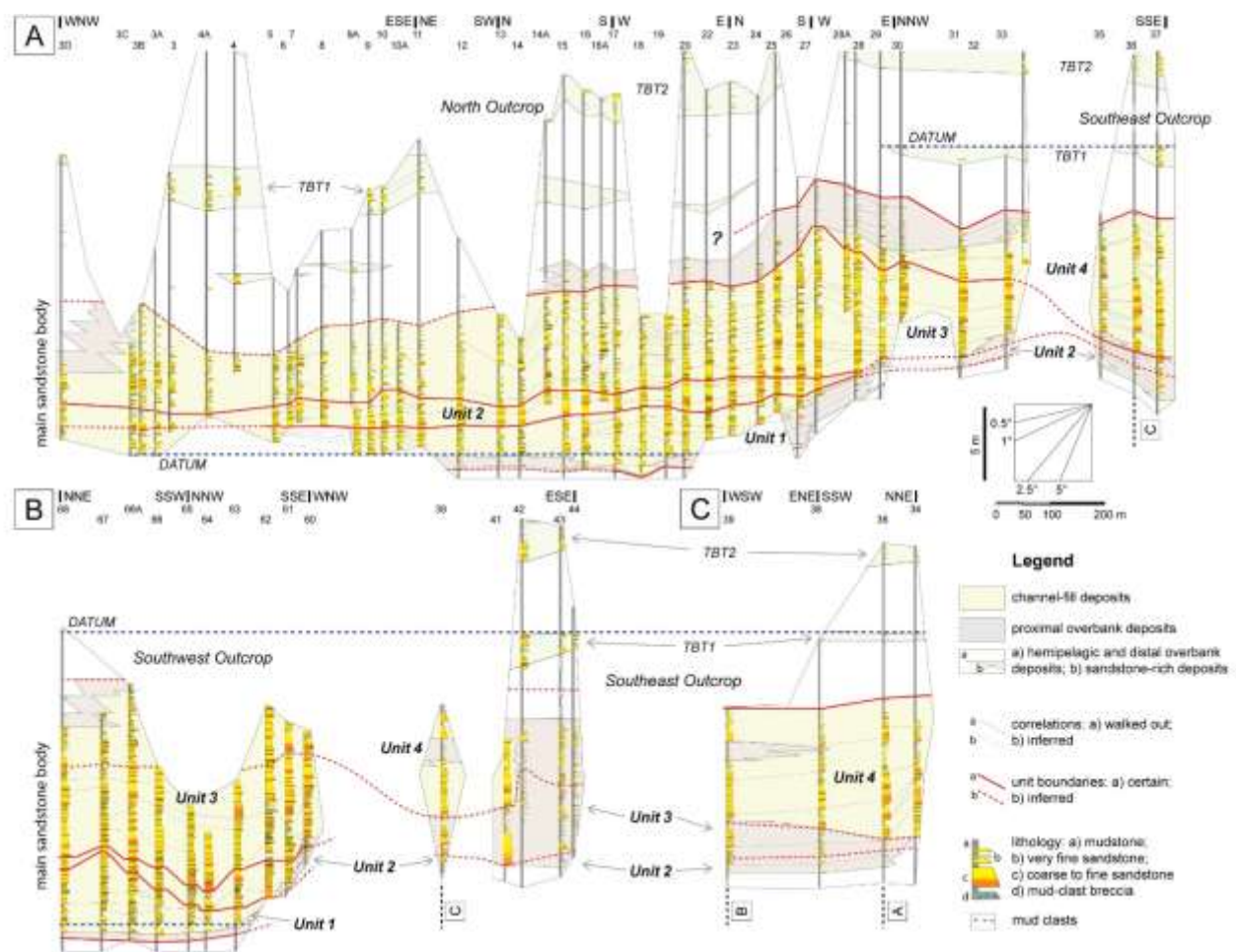


Fig. 3. A–C) Correlation panels (location shown in Fig. 2A) relating the deposits of channel–levee Complex 5 exposed in the North Outcrop, the Southwest Outcrop, and the Southeast Outcrop and showing the gross stratigraphic and spatial distribution of channelized vs. overbank deposits and the boundaries of the four stratigraphic units defined in this study.

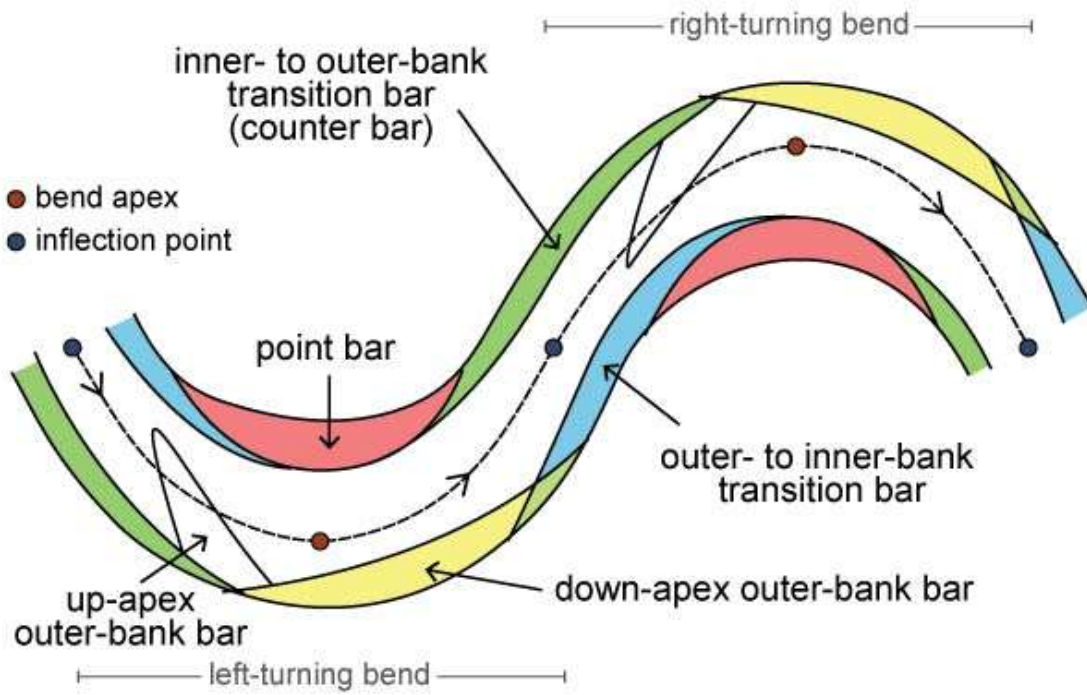


Fig. 4. Terminology of channel bars and channel bend regions used in the present paper (modified after Janocko et al., 2013b).

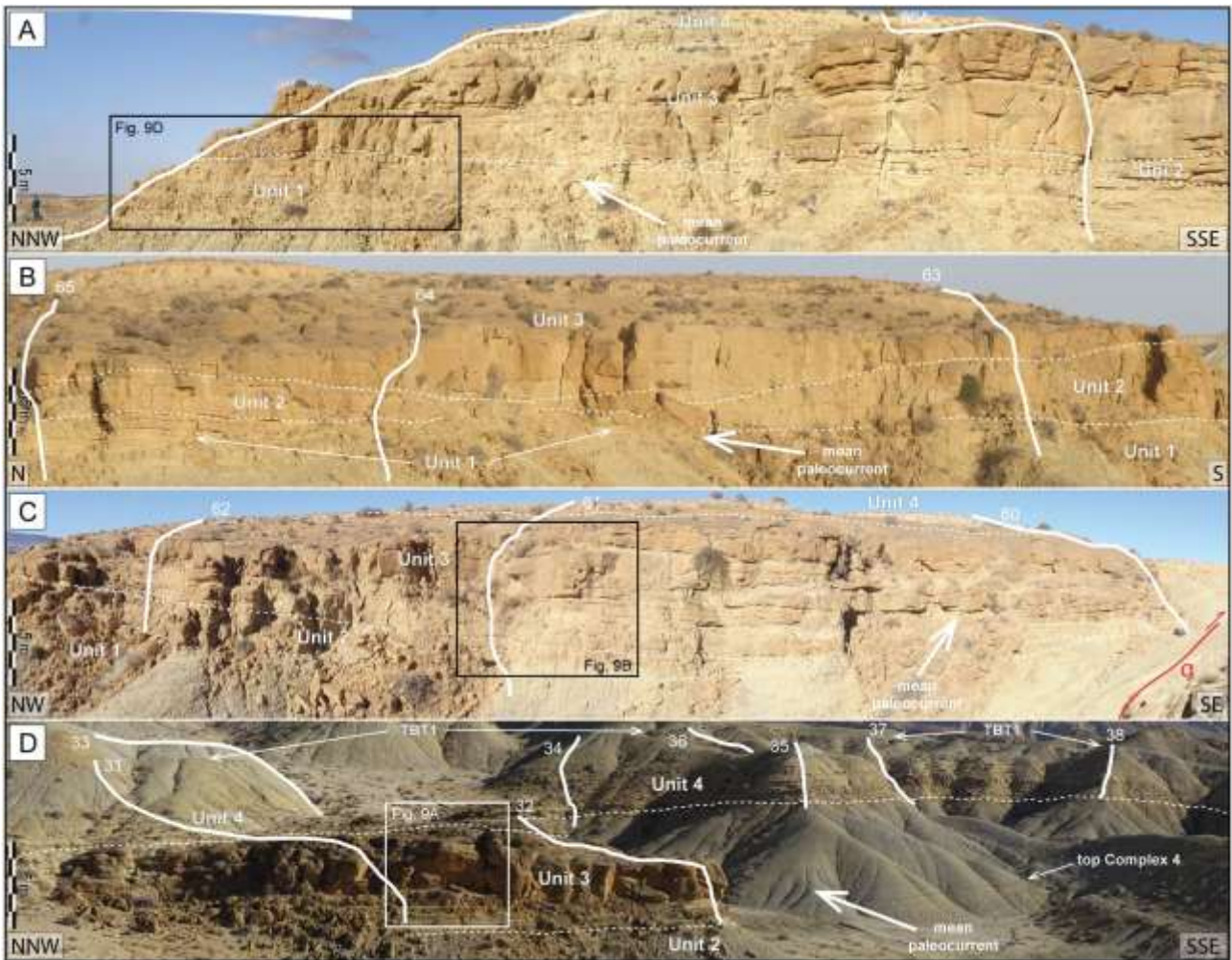


Fig. 5. Panoramic photographs of (A–C) the Southwest Outcrop and (D) the southeasternmost part of the North Outcrop (foreground) and the Southeast Outcrop (background), with location of sedimentary logs shown in Fig. 3.

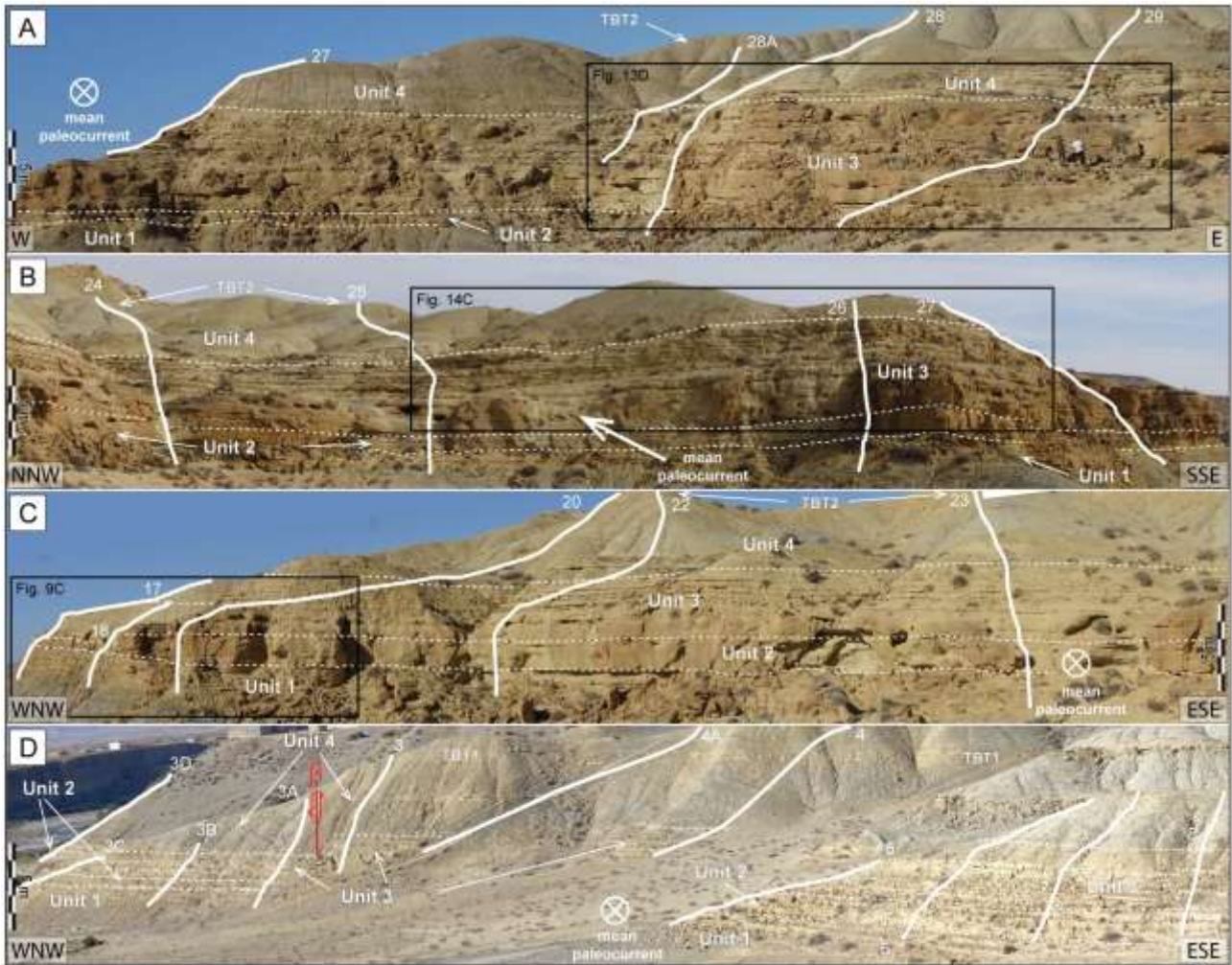


Fig. 6. A–D) Panoramic photographs of the North Outcrop, proceeding from (top to bottom) the southeast to the northwest, with location of sedimentary logs shown in Fig. 3.

| Facies name | Grain Size and Sorting | Sedimentary Structures and Bioturbation | Bed Thickness Range (cm) | Upper and Lower Contacts | Process Interpretation | Facies Equivalents |
|---|---|--|--------------------------|---|--|--|
| F1 Mud-clast-rich coarse sandstone | Upper-medium to very coarse sand; mud clasts are up to fine cobble, subrounded; basal lags up to fine pebbles; poorly sorted | Crude normal grading, coarser lags in basal scours; inversely graded sand to granule layers close to bed base, abundant mud clasts dispersed or concentrated in the lower or in the upper part of beds, randomly oriented | 35–70 | Sharp, erosional lower, with flute and groove casts, or gradational lower from F2; sharp upper or gradational upper with F4 | Traction-carpet and en-masse (suspension) deposition from high-density turbidity currents | S1–S3 of Lowe (1962); F4 and F6 of Mutti (1992) |
| F2 Mud-clast breccia | Mud clasts up to very coarse pebble, subangular to moderately rounded; matrix is upper-medium to very coarse sand, very poorly sorted | Mud clasts randomly oriented | 5–25 | Sharp, erosional lower, often with basal scours up to c. 1 m deep and a few tens of m, sharp upper or gradational upper with F1 | Freezing of a mud-clast-rich traction carpet developed at base of high density flows, following interaction with the mud-rich internal levee | |
| F3 Cross-stratified medium sandstone | Lower-medium to lower-coarse sand; mud clasts are granule to medium pebble, moderately sorted | Crude normal grading, low-angle cross-lamination; bioturbation moderate to absent, in the upper parts of beds | 30–55 | Sharp, erosional lower, sharp upper | Traction-deposition from high-density turbidity currents | Tt of Lowe (1962); F6 of Mutti (1992) |
| F4 Structureless medium-fine sandstone | Upper-fine to lower-medium sand, coarser lags at base of beds, moderately well-sorted | Crude normal grading, inversely graded layers close to base of beds; rare mud clasts, concentrated in the lower or in the upper parts of beds, randomly oriented; bioturbation moderate to absent, in the upper part of beds | 5–15 | Sharp, erosional lower, with flute and groove casts; sharp upper or gradational upper with F5 | En-masse (suspension) and traction-carpet deposition from high-density turbidity currents | T ₁ division of Bouma (1962); S2–S3 of Lowe (1962); F7 and F8 of Mutti (1992) |
| F5 Laminated fine-very fine sandstone | Very fine to upper-fine sand, well-sorted | Normal grading, planar-parallel, and ripple lamination; convolutions; bioturbation intense | 1–5 | Sharp lower, sharp upper or gradational upper with F8 | Traction-plus-fallout deposition from waning low-density turbidity currents | T ₂ sequence of Bouma (1962) |
| F6 Turbidite mudstone | Clay to silt | Fairly laminated | 1–60 | Sharp lower or gradational lower from F5; sharp upper or gradational upper with F7 | Fallout from very diluted turbidity currents | T ₃ Bouma (1962) division |
| F7 Maristone | | Contains test of pelagic foraminifera and fragments of thin-shelled mollusca | | Gradational lower from F6 | Hemipelagic fallout | |

Table 1. Sedimentary facies recognized in the studied part of channel–levee Complex 5.

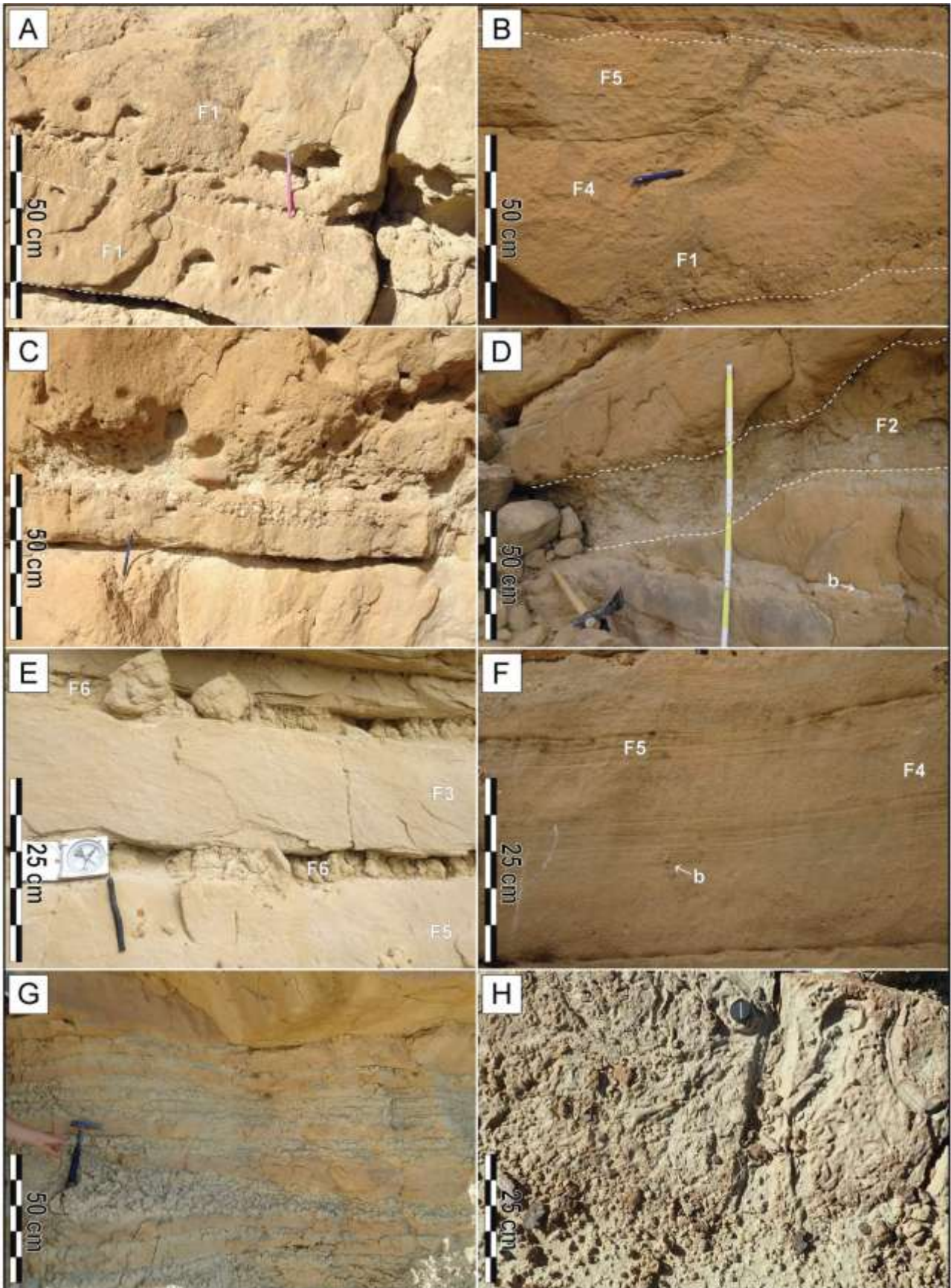


Fig. 7. Selected field photographs of sedimentary facies described in Table 2. A) Crudely graded, mud-clast-rich coarse sandstones (F1). Note the numerous pebble-size mud clasts close to the bed

base (dashed with line). B) Normally graded sandstone bed composed of a lower poorly sorted division (F1) with mud clasts and poorly developed inversely graded layers, a middle massive interval (F4), and a relatively thick planar-parallel-laminated top (F5). C) Basal lag with pebbles and cm-size mud clasts at the base of a coarse sandstone bed (F1). D) Mud-clast breccia (F2), lining up an erosional surface. Note the presence of burrows (*b*) in the fine-grained tops (F5 and F6) of the sandstone beds below. E) Alternation of laminated fine sandstones (F5), cross-stratified medium sandstones (F3), and turbidite mudstones (F6). F) Amalgamated sandstone beds made up of a lower normally graded massive division (F4) and a laminated upper division (F5). G) Normally graded very fine sandstone beds (F5) capped by turbidite mudstones (F6). H) Highly bioturbated top of a sandstone bed of Facies 5 with well-preserved burrows.

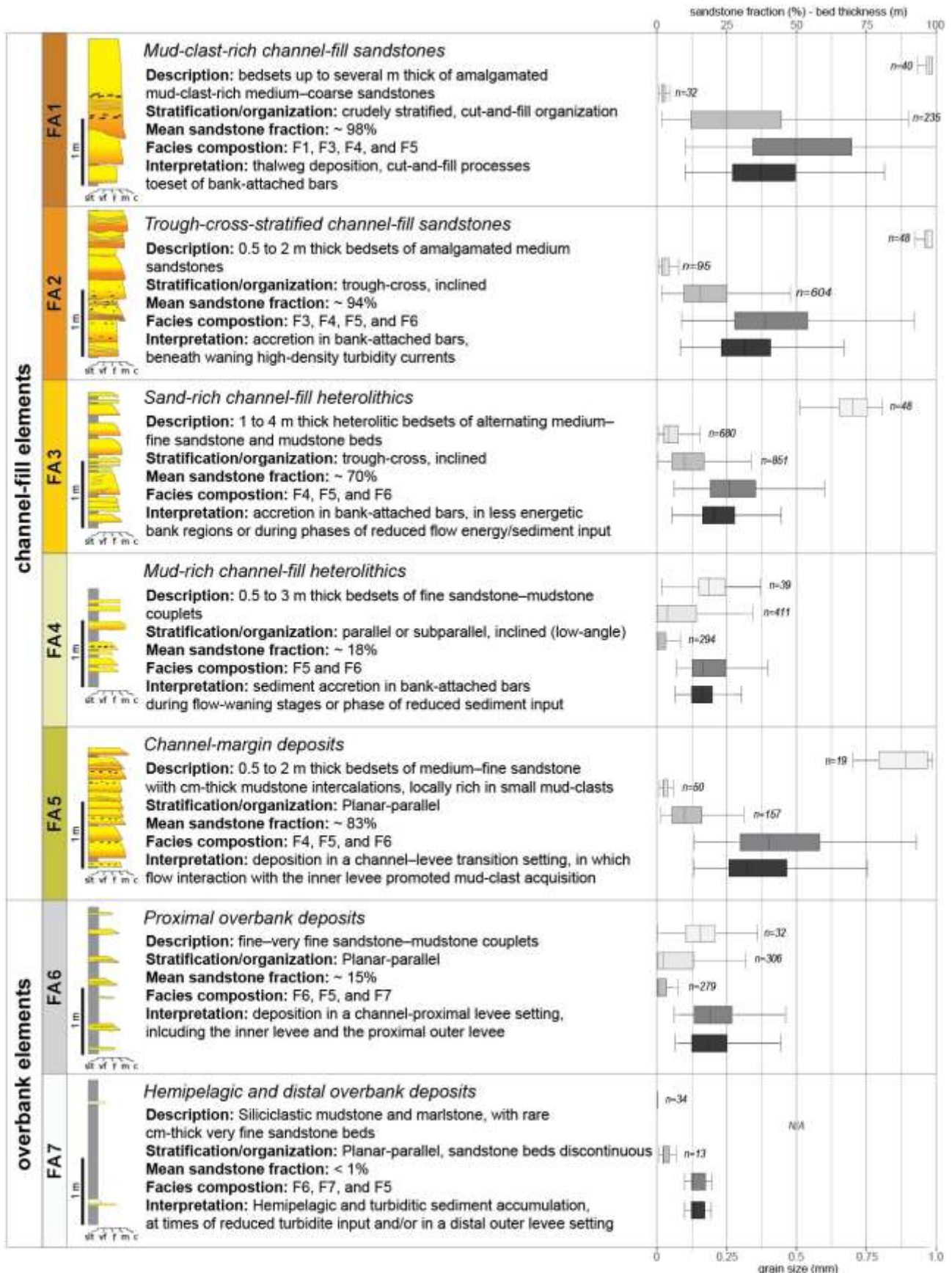


Fig. 8. Facies associations recognized in Complex 5. For each facies association (FA) the statistical distribution, based on n observations of (from top to bottom, in different gray tones), the sandstone

fraction (as a percentage, top axis), thickness (in centimeters, top axis) of mudstone and sandstone beds, and mean and basal sandstone grain size (in millimeters, bottom axis) is shown as box plots, in which boxes contain the 25th to 75th percentiles, the line in the box is the median value, and whiskers mark the 5th and 95th percentiles,. The generally poorly exposed nature of FA7 makes it difficult to determine mudstone-bed thickness, which are thus not shown.

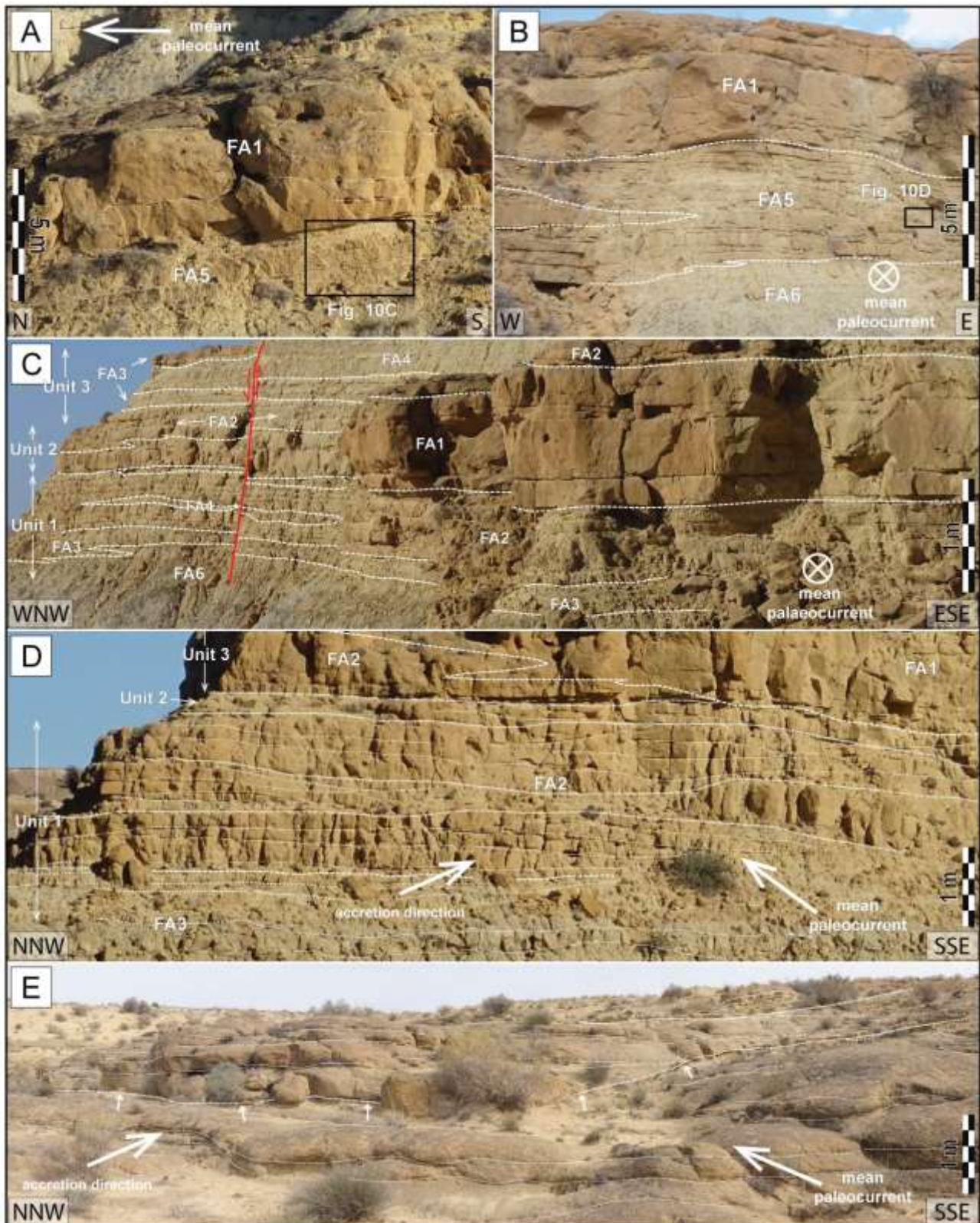


Fig. 9. Selected field photographs of facies associations. Dashed lines are facies association (FA) boundaries. Zig-zag FA boundaries mark gradational lateral transitions. A) The channel-fill amalgamated sandstones of FA1 in the North Outcrop (location shown in Fig. 5D), overlying the

channel-margin deposits of FA5. Dotted lines highlight the inclined stratification, dipping towards the right and the southeast. B) View of the Southwest Outcrop between logs 60 and 61 (location shown in Fig. 5C), showing the eastward transition from the amalgamated sandstone of FA1 to the less amalgamated channel-margin sandstones of FA5. C) View of the North Outcrop (location shown in Fig. 6C) illustrating the scale of facies association heterogeneity. D) The Southwest Outcrop at log locality 67 (location shown in Fig. 5A). The bold dotted lines are boundaries of co-directional bedsets. Note the lateral transition from FA1 to FA2 in the upper part of the cliff. E) Favorable exposure (Southwest Outcrop, between log localities 66-67) oblique to stratification showing the complex internal organization of FA2 bedsets. Arrows highlight a scoured bedset base.

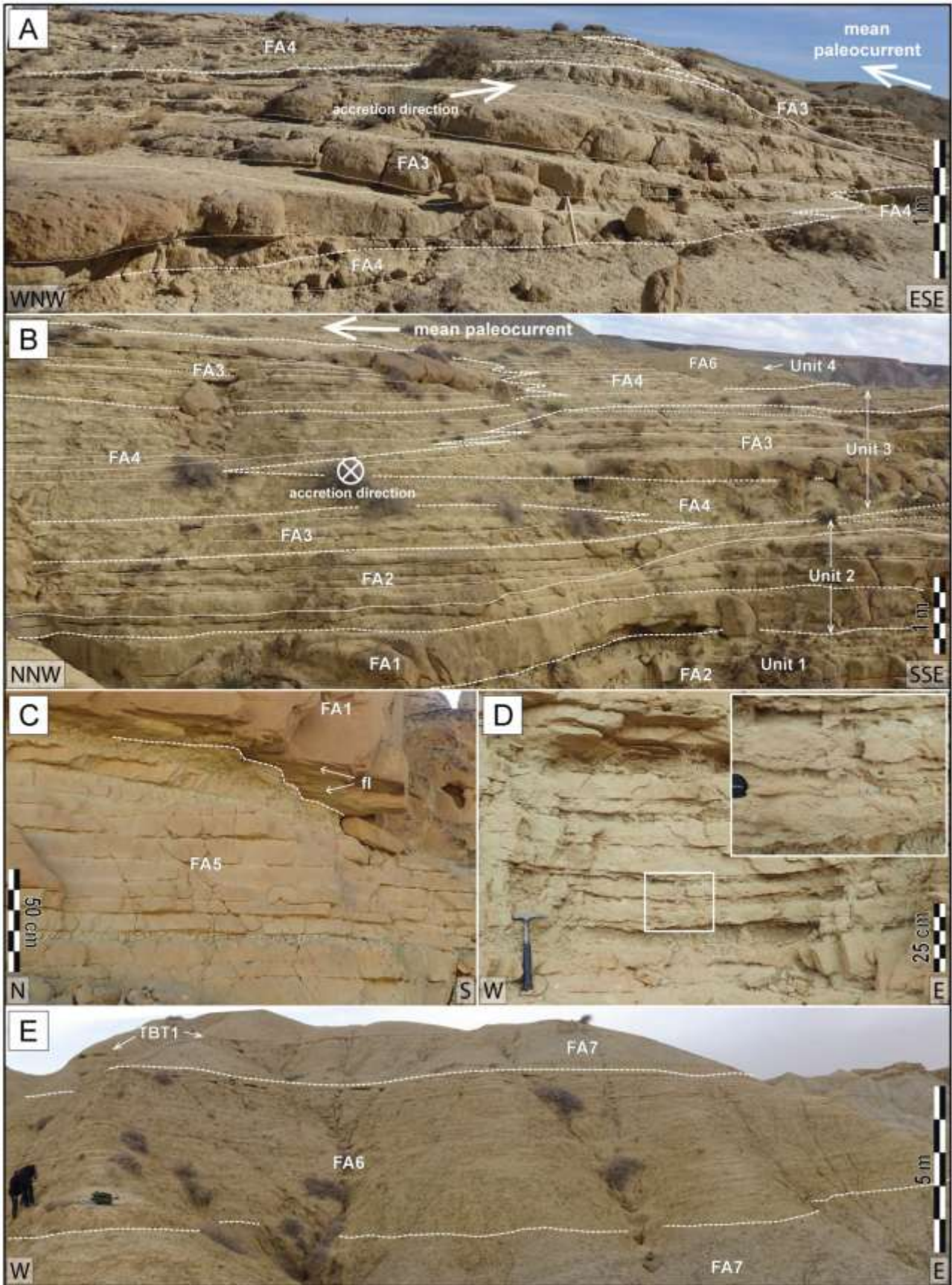


Fig. 10. Selected field photographs of facies associations. Dashed lines are facies association (FA) boundaries. Zig-zag FA boundaries mark gradational lateral transitions. A) Laterally accreted

bedsets of Unit 3 between log localities 17 and 18. Note the along-accretion dip transition from the sand-rich FA3 and the mud-rich FA 4. B) Facies association composition of Unit 2 and Unit 3 in the North Outcrop, between log localities 16 and 17. Note the gradational lateral transitions between FA3 to FA4, and the overall trough-cross-stratified character of the deposit. D–E) The amalgamated to non-amalgamated sandstones of FA5 (location shown in Figs. 9A, B). D) Note the presence of small north-directed flute casts (fl) at the base of FA1. F) Proximal overbank deposits of FA6 of Unit 4 between log localities 43 and 44, sandwiched by the mudstones of FA7.

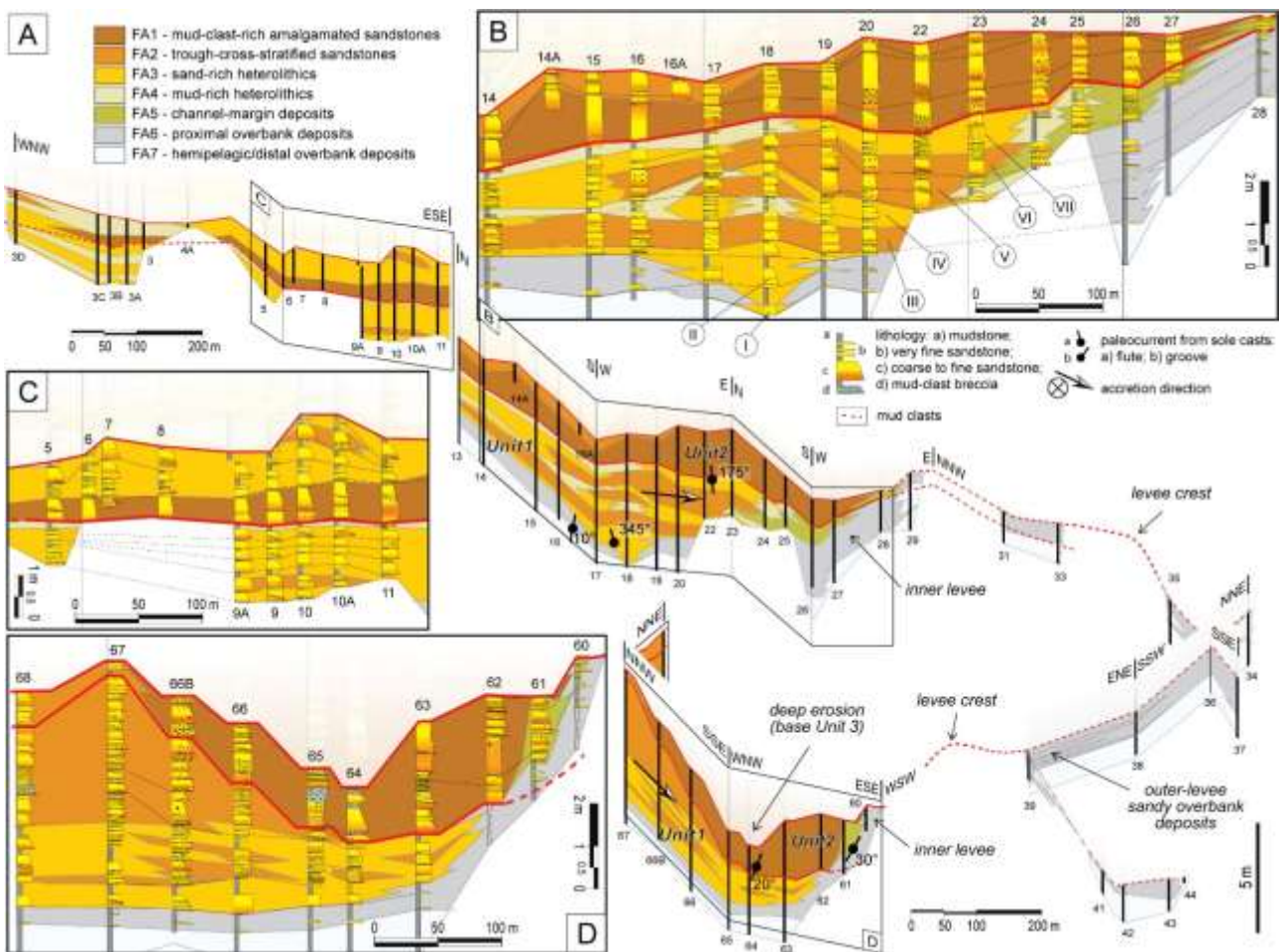


Fig. 11. A) Fence diagram of Unit 1 and Unit 2 (35 x vertical exaggeration; location shown in Fig. 2A) illustrating the spatial distribution of channel-fill vs. overbank facies associations, with details (B–D) showing sedimentary logs and correlations from key exposures.

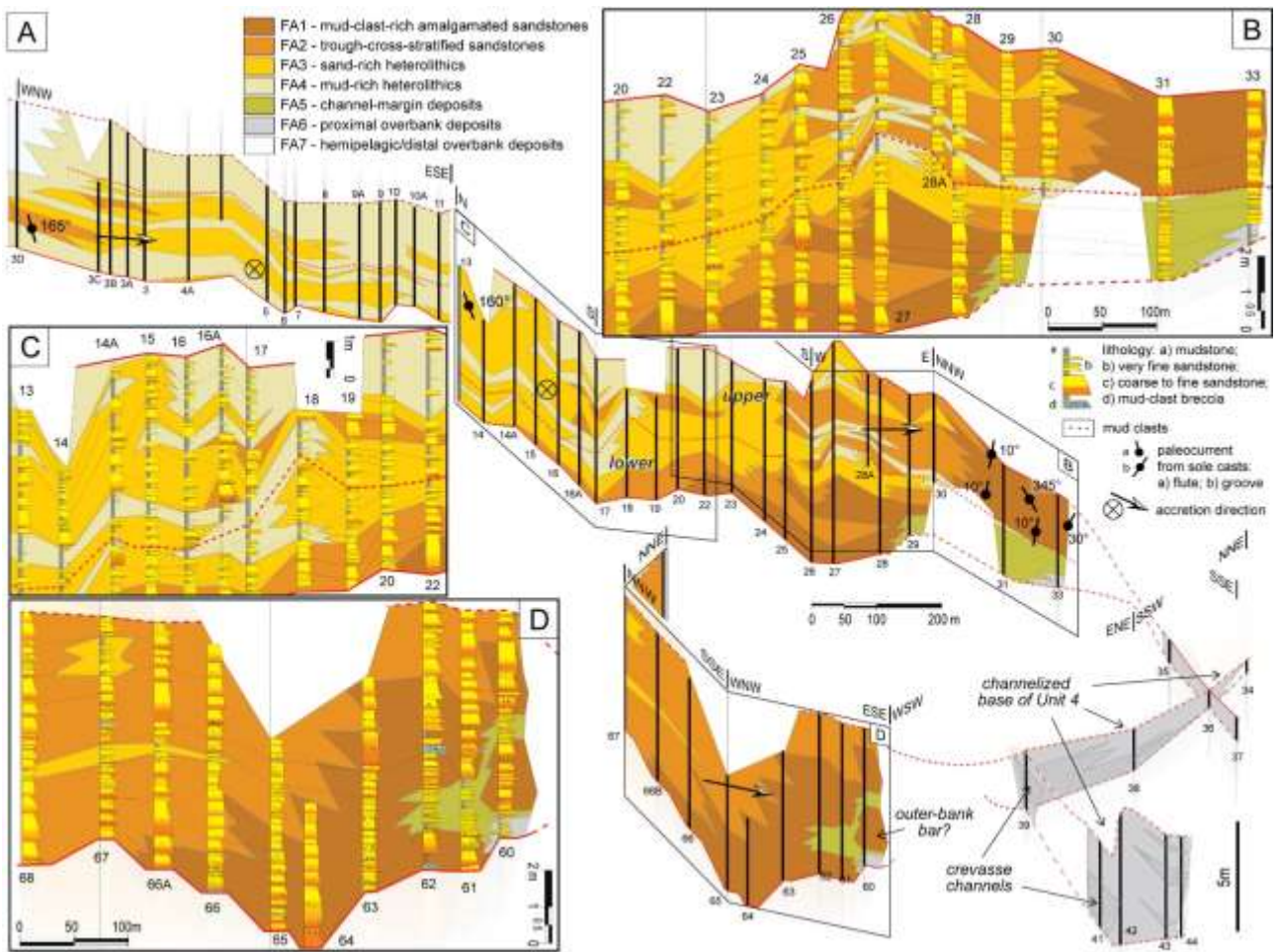


Fig. 12. A) Fence diagram of the lower and the upper parts of Unit 3 (35 x vertical exaggeration; location shown in Fig. 2A) illustrating the spatial distribution of channel-fill vs. overbank facies associations, with details (B–D) showing sedimentary logs and correlations from key exposures.

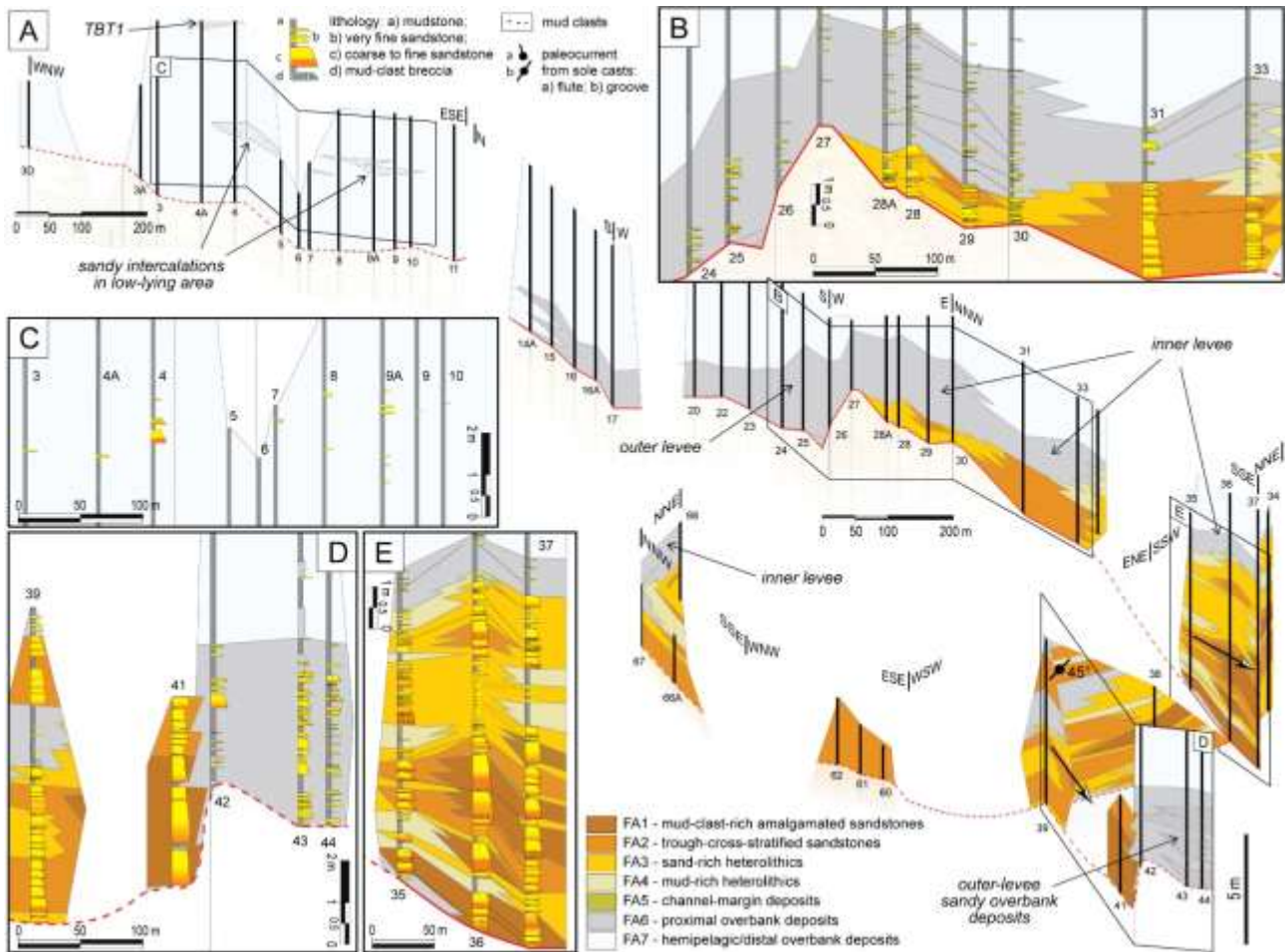


Fig. 13. A) Fence diagram of Unit 4 (35 x vertical exaggeration; location shown in Fig. 2A) illustrating the spatial distribution of channel-fill vs. overbank facies associations, with details (B–D) showing sedimentary logs and correlations from key exposures.

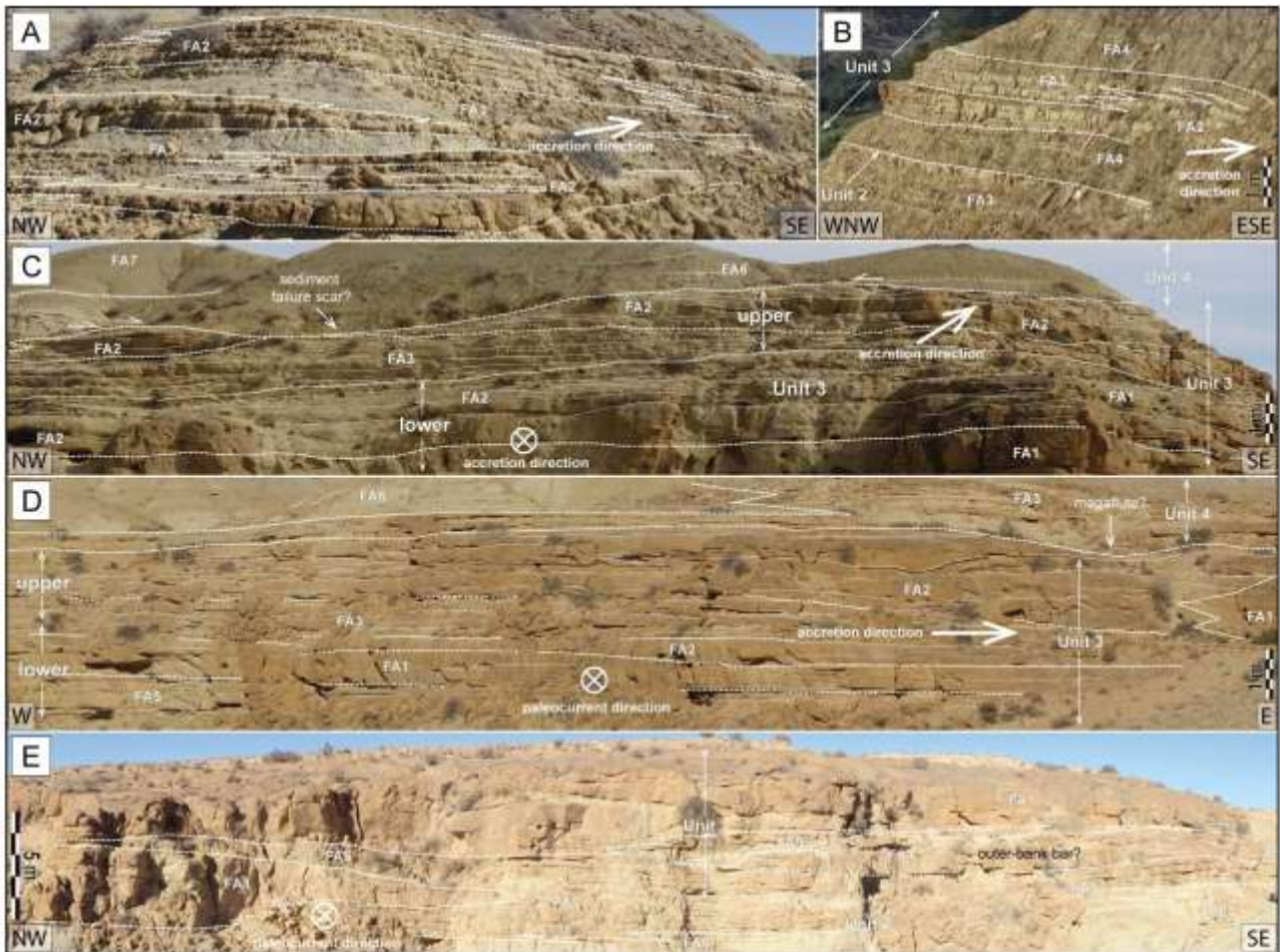


Fig. 14. Selected field photographs of key exposures, with facies-association (FA) boundaries (dashed lines). Zig-zag FA boundaries are gradational lateral transitions. Laterally accreted bedsets in the lower Unit 3 at log locality 5 (A) and log locality 3D (B). Unit 3 to the north (C) and to the east (D) of log locality 27 (location shown in Figs. 6A, B), with hand drawings highlighting the laterally accreted nature of the deposits. E) Panoramic view of the Southwest Outcrop showing the transition from the channelized FA1 and FA5 to the proximal overbank deposits of FA6. Note the presence of the FA1 amalgamated sandstones on the right-hand side of the picture, likely representing an outer-bank bar deposit.

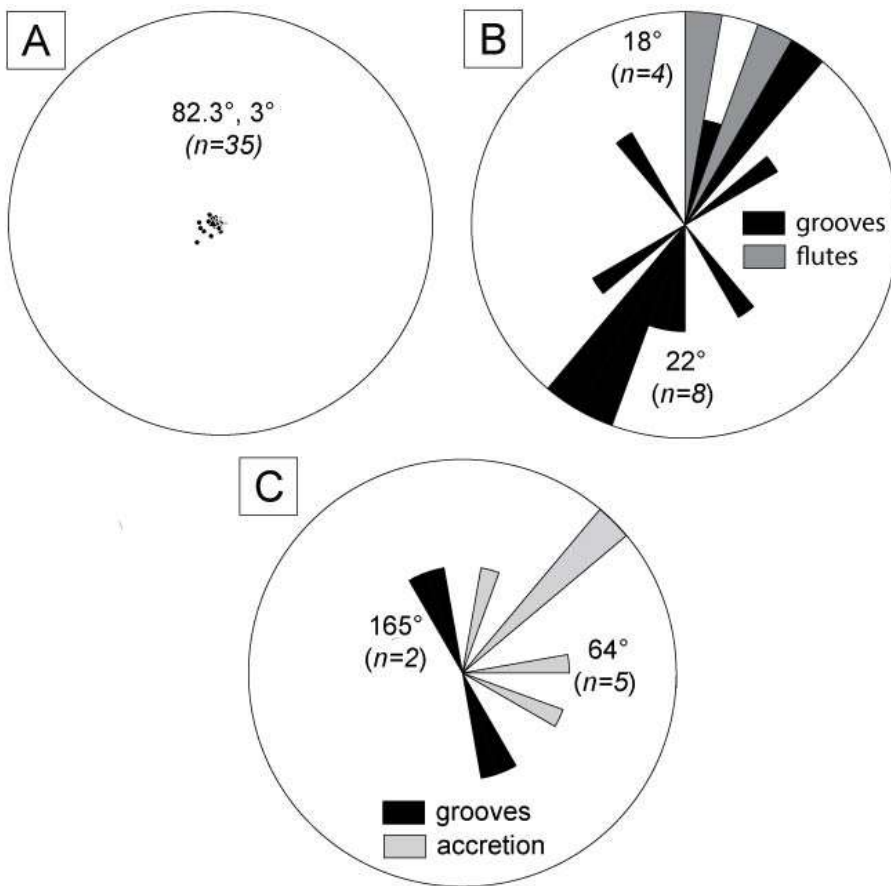


Fig. 15. Equal-area projection (lower-hemisphere) plot of poles to planes of tilt-corrected internal bedding of a laterally accreted bedset from the upper Unit 3. B) Rose plot showing the orientation of sole casts from logs 31-33, with mean values. C) Rose plot of groove-mark orientation and accretion direction from localities 15–17, with mean values.

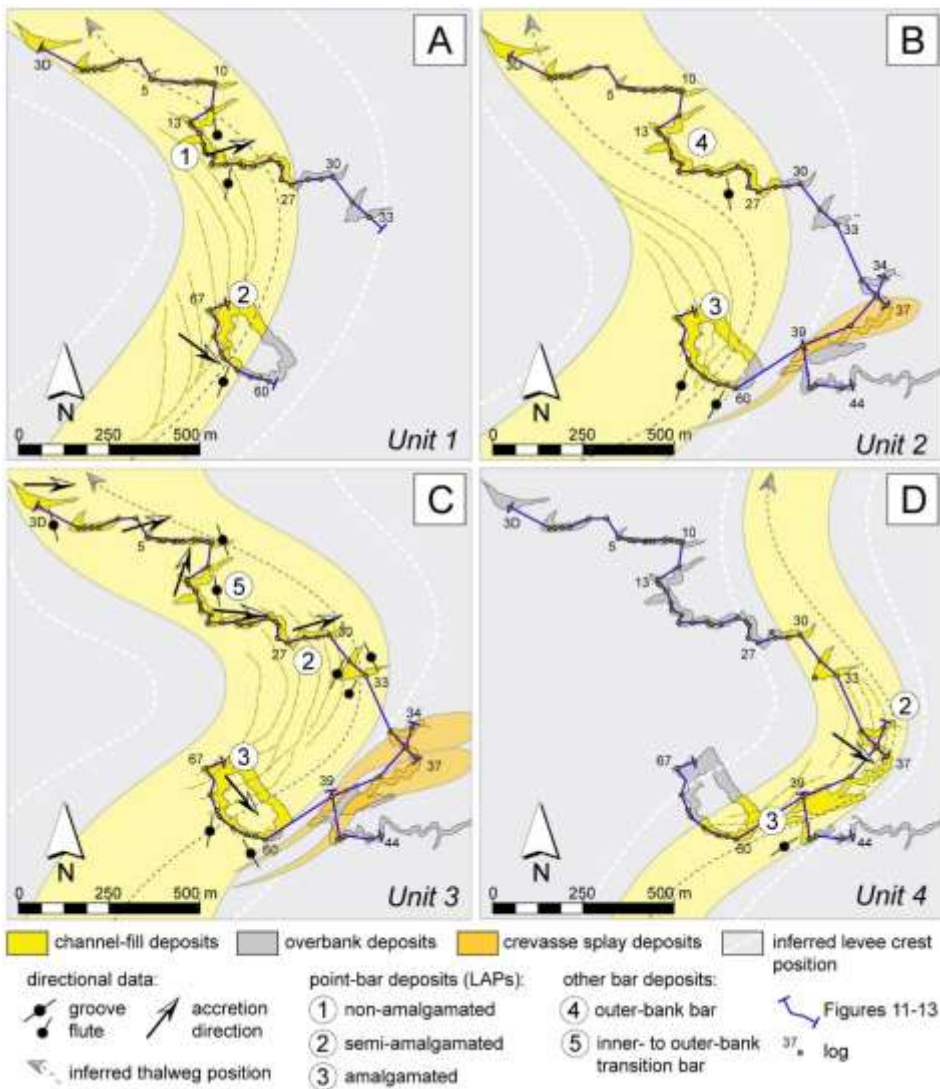


Fig. 16. A–D) Idealized maps of Units 1 to 4, reconstructed from facies-association distribution and direction data, showing the channel pathway and showing the occurrence of the recognized bar deposits. LAP types are after Abreu et al. (2003).

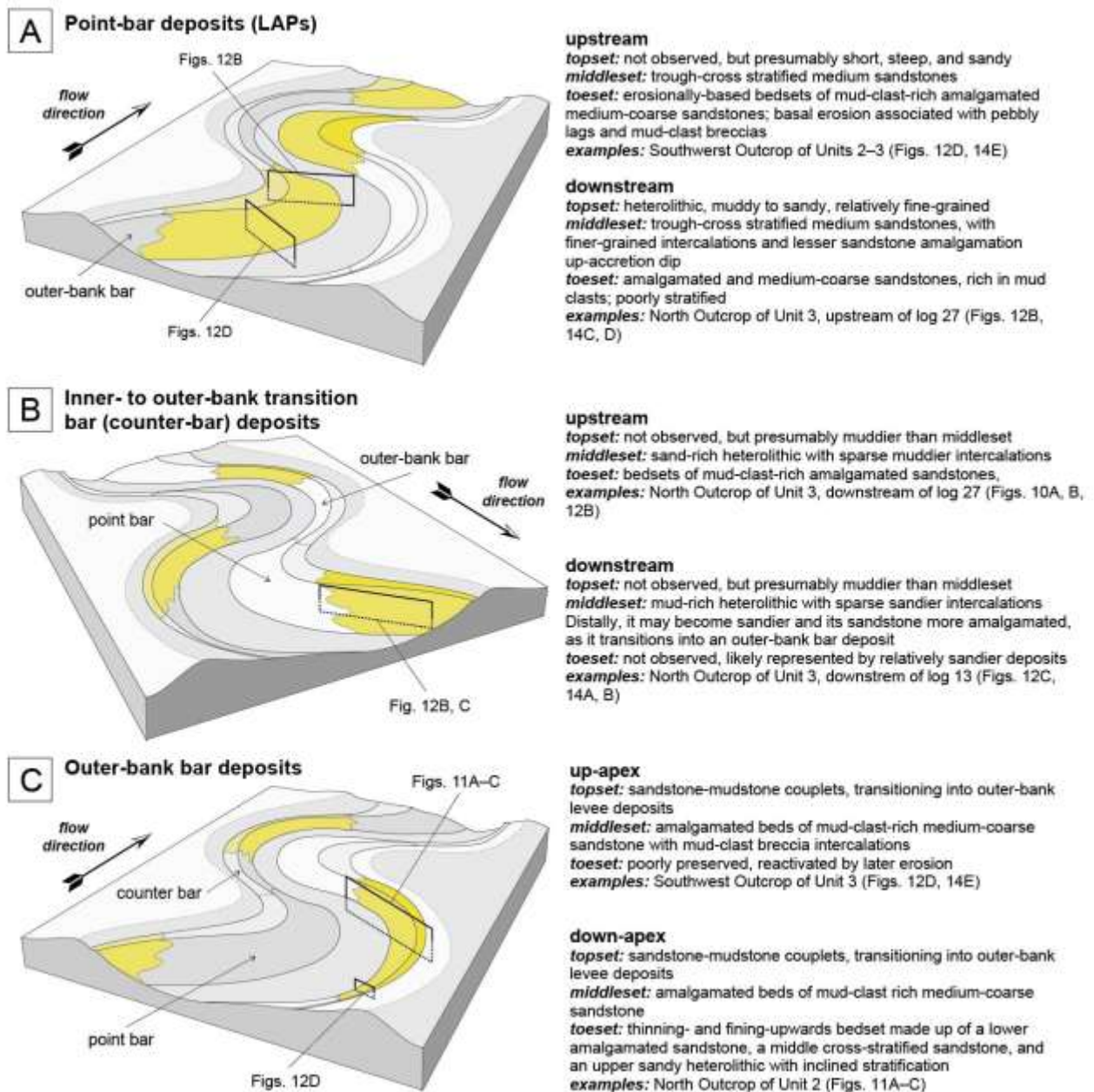


Fig. 17. Salient characteristics of A) point-bar, B) inner- to outer-bank transition bar (counter-bar), and C) outer-bank bar deposits recognized in Complex 5, with schematic block diagrams (sides are approximately 1 km long; modified after Janocko et al. 2013b) showing their likely occurrence relative to bend apexes and inflection point. The bar type in question for each figure part is highlighted in yellow.